Szymon Gamrat

Student's number: 1154543

Studies of control samples and backgrounds for the measurement of direct CP violation with interferometric methods at KLOE

Master's thesis
in the field of experimental physics

Thesis created under
the supervision of dr Eryk Czerwiński

Department of Experimental
Particle Physics and Applications

Cracow 2023

Contents

Abstrakt

Głównym celem poniższych studiów jest wyznaczenie poprawki do wydajności selekcji pod hipotezą $\mathrm{K_S K_L} \to \pi^+\pi^-\pi^0\pi^0$ uzyskanej z Monte Carlo. Użyto do tego eksperymentalnie zebranej próbki danych, a wydajność znaleziono w funkcji różnicy czasów własnych kaonów Δt w momentach ich rozpadów. Praca stanowi kontynuację analizy prowadzącej do zdeterminowania parametrów łamania symetrii CP $\mathrm{Re}(\varepsilon'/\varepsilon)$ i $\mathrm{Im}(\varepsilon'/\varepsilon)$ rozpoczętej w [1].

Zasada pomiaru jest oparta na selekcji kanałów tła mających własności wspólne z $\mathrm{K_S K_L} \to \pi^+\pi^-\pi^0\pi^0$. Wybranymi rozpadami są $\mathrm{K_S K_L} \to \pi^\pm \mathrm{l}^\mp \nu \pi^0\pi^0$, $\mathrm{K_S K_L} \to \pi^+\pi^- 3\pi^0$ oraz $\mathrm{K_S K_L} \to \pi^+\pi^-\pi^+\pi^-$, które odpowiadają rozpadom $\mathrm{K} \to \pi^0\pi^0$ i $\mathrm{K} \to \pi^+\pi^-$ występującym w sygnale.

Pierwszym krokiem był o wykonanie selekcji pod hipotezą każdego z rozpadów tagujących ($\mathrm{K} \to \pi^\pm \mathrm{l}^\mp \nu$, $\mathrm{K_L} \to 3\pi^0$ albo $\mathrm{K_S} \to \pi^+\pi^-$) i osiągnięcie najwyższej możliwej czystości próbki. Póniej liczba zdarzeń tagujących była ważona poprzez stosunek rozgałęzie odpowiedniego rozpadu znajdującego się w sygnale, aby otrzymać tak zwaną oczekiwaną dystrybucję różnicy czasów rozpadów. Dodatkowa selekcja pod hipotezą $\mathrm{K} \to \pi^0\pi^0$ albo $\mathrm{K} \to \pi^+\pi^-$ była nakładana na zdarzenia po selekcji tagującej w celu uzyskania próbki naśladującej wyselekcjonowaną dla $\mathrm{K_S K_L} \to \pi^+\pi^-\pi^0\pi^0$ przy użyciu MC. Co ważne, zachowana musiała być niezależność rekonstrukcji między rozpadami naładowanymi i neutralnymi, więc do ustalenia wierzchołka neutralnego zaadaptowano metodę trilateracji. Ostatecznie, mając wyznaczone zarówno oczekiwane i wyselekcjonowane dystrybucje Δt zdeterminowano poprawkę do wydajności poprzez podzielenie wydajności uzyskanej z danych przez wydajność z Monte Carlo. Wynik nie jest rozkładem jednorodnym, więc w istocie każdemu podprzedziałowi histogramu Δt odpowiada specyficzny czynnik. Niepewności wyznaczone zostały za pomocą standardowej propagacji niepewności pomiarowej. Wyznaczona poprawka zostanie użyta w dalszych studiach nad łamaniem symetrii CP w układach kaonów splątanych.

Abstract

The main goal of these studies is to determine a correction factor for the efficiency of selection obtained using $\mathrm{K_S K_L} \to \pi^+\pi^-\pi^0\pi^0$ Monte Carlo events using experimentally collected data in the function of time difference Δt between decays of kaons. It constitutes a continuation of an analysis for $\mathrm{Re}(\varepsilon'/\varepsilon)$ and $\mathrm{Im}(\varepsilon'/\varepsilon)$ parameters, which began in [1].

Measurement principle is based on the selection of background channels having common properties with $\mathrm{K_S K_L} \to \pi^+\pi^-\pi^0\pi^0$. The chosen decays were $\mathrm{K_S K_L} \to \pi^\pm \mathrm{l}^\mp \nu \pi^0\pi^0$, $\mathrm{K_S K_L} \to \pi^+\pi^- 3\pi^0$ and $\mathrm{K_S K_L} \to \pi^+\pi^-\pi^+\pi^-$ corresponding to signal-like parts $\mathrm{K} \to \pi^0\pi^0$, $\mathrm{K} \to \pi^+\pi^-$, respectively.

The first step was to perform a selection under the hypothesis of each tagging decay ($\mathrm{K} \to \pi^\pm \mathrm{l}^\mp \nu$, $\mathrm{K_L} \to 3\pi^0$ or $\mathrm{K_S} \to \pi^+\pi^-$) and reach the highest possible purity. Then, the number of tagging events was weighted with a branching ratio for each signal-like part to obtain so-called expected distributions of the time difference. The additional selection under the hypothesis of $\mathrm{K} \to \pi^0\pi^0$ or $\mathrm{K} \to \pi^+\pi^-$ was imposed on the events after tagging to mimic the selection performed for $\mathrm{K_S K_L} \to \pi^+\pi^-\pi^0\pi^0$ using MC. Importantly, independence between charged and neutral parts of decay had to be conserved, so the method of trilateration was adapted to reconstruct a neutral vertex. Finally, having determined the expected and selected distributions of Δt, a correction factor can be calculated via the division of efficiency obtained from data by the efficiency from MC. The result is not a uniform distribution, so there exists a specific factor for each bin of the Δt histogram. Final uncertainties were determined using a standard propagation of a measurement error. A measured correction will be used in the further studies over CP symmetry breaking in the entangled kaons' systems.

1 Introduction

1.1 Physical transformations

Physical transformations are the operations developed in the mathematical formalism. They correspond to the change of variables of wave functions or observables themselves and can be divided into independent types, which are extensively described below.

The continuous transformations correspond to the operations tied with classically understood physical reality, like spatial translation or rotation of a system. Its action on wave functions can be reached by the elements $\hat{U}$ of certain Lie groups dependent on continuous parameters $\theta(x)$, noted in general as:

$$\hat{U} = \exp\left(i[\theta(x)]_a \hat{T}^a\right), \tag{1.1}$$

where $\hat{T}^a$ is a-th generator of a given Lie group and $[\theta(x)]_a$ - a-th component of parameters vector. They are unitary by definition, so cannot lead to the change in the result of a measurement of observables. If parameters are dependent on a spacetime point, the transformations are called *local*, while for independent - *global*. Local transformations specify the gauge independence of the theory and forms of all its derivatives, e.g., field strength tensor. The significance of global ones is magnified by *Noethers theorem* (firstly proved in [2]), which states that each conserved global symmetry generates a conservation law and a conserved current. An example could be the invariance of QED with respect to U(1), which proves charge conservation and form of QED probability current. Despite their importance, these transformations are not directly studied in the thesis.

Discrete symmetry is represented by the operator $\hat{A}$ having a property:

$$\hat{A}\hat{A} = \alpha \mathbb{1}, \tag{1.2}$$

where $\mathbb{1}$ is an identity and α - complex number of unit magnitude. Obviously, acting twice with a given operator leaves the state unchanged. These symmetries can be determined from measurable, intrinsic characteristics of a system, e.g., differential cross-section. More general theory of symmetry operators allows stating, that with a suitable phase convention every discrete operator is linear and unitary or anti-linear and anti-unitary [3]. As was mentioned before, unitary ones are responsible for the conservation laws, which in this case are decay selection rules and superselection rules like law of conservation of statistics. There are three distinguished elementary transformations, out of which two will have a notable importance for the reader.

First is known as *parity*, P, an operation defined by the inversion of three spatial coordinates of a wave function, $x \to -x$, $y \to -y$, $z \to -z$, which leads, as well, to the

transformation of position and momentum observables in a way:

$$\begin{aligned} \hat{P}\hat{\mathbf{r}}\hat{P}^{-1} &= -\hat{\mathbf{r}}, \\ \hat{P}\hat{\mathbf{p}}\hat{P}^{-1} &= -\hat{\mathbf{p}}. \end{aligned} \tag{1.3}$$

Such a symmetry is certainly violated in weak interactions - first recognition in β decay of ${}^{60}_{27}Co$ [4], which lead to their theoretical description of weak interactions by V-A term in Standard Model Lagrangian [5].

The second transformation is called *charge conjugation*, C, which replaces charge Q, hypercharge Y, baryon number B and two lepton numbers L_e and L_μ with corresponding opposites (particle-antiparticle interchange). Moreover, by quark SU(3) model, these quantities can be tied with strangeness S and isospins z-component I_z by relations:

$$\begin{aligned} S &= Y - B, \\ I_z &= Q - \frac{1}{2}Y, \end{aligned} \tag{1.4}$$

so conjugation of these numbers is obvious in this notation. Charge conjugation is not an exact symmetry of nature, which was proved in the experiment [6], which observed inverted helicity of positrons with respect to electrons coming from muon decays.

A third operation, known as *time reversal* T, leads to the inversion of the time component in wave functions, but the corresponding operator is anti-linear and anti-unitary. Invariant quantities under its action are helicity $\hat{\sigma} \cdot \hat{\mathbf{p}}$ and position $\hat{\mathbf{r}}$, while momentum $\hat{\mathbf{p}}$, orbital angular momentum $\hat{\mathbf{L}}$ and spin $\hat{\sigma}$ are inverted. Most of the other observables are in fact left unchanged. Its anti-unitarity eliminates the possibility of a conservation law, but squared time reversal TT leads in fact to the law of conservation of statistics. The proof can be found, for example, in [3].

Moreover, action of discrete operators can be joint, so that more complex symmetries can be studied as well. The most important for todays understanding of Standard Model physics is CPT symmetry, which still seems to be an exact symmetry of nature. The most constraining results are extracted from neutral kaons systems and can be found in [7]. The greatest importance for this thesis, however, will have a CP transformation, being under the constant examination since 1960s. It will be discussed more extensively in the next subsection. T symmetry violation was shown for B^0 system by BaBar collaboration [8], while no violation was noticed for K^0 system by KLOE-2 collaboration (preprint of [9] submitted to peer-review).

1.2 CP violation in quark sector

CP transformation is a sequential action of parity and charge conjugation operators on a quantum state. From a classical intuition there is no reason for the violation of this

symmetry and this is proved for strong interactions and electromagnetism. First premises about its breaking came by studies of β-decay:

$$n \to p + e^- + \overline{\nu}_e, \tag{1.5}$$

for which experimentally found weak interactions' strength was systematically smaller than for purely leptonic one:

$$\mu \to e + \nu_e + \overline{\nu}_\mu. \tag{1.6}$$

Proof of CP symmetry violation was, however, established in the experiment of James Cronin and Val Fitch (1964) regarding neutral kaons [10], for which the Nobel Prize 1980 was awarded.

The first theoretical description approach was taken in 1963 by Nicola Cabibbo through the assumption of a so-called Cabibbo matrix in [11], which lead to (u,d,s) quark doublets with mixed down and strange quarks in the second component. It fixed the problem with Fermis constant incompatibility within the theory, but generated the problem of non-observed flavor changing neutral current in weak interactions. It exposed itself in strange mesons' branching ratios' asymmetry:

$$\frac{BR[K^+ \to \pi^+ + \nu + \overline{\nu}]}{BR[K^+ \to \pi^0 + \mu^+ + \overline{\nu}_\mu]} \leq 10^{-5}. \tag{1.7}$$

The problem was finally resolved by the introduction of c quark (charm) by Glashow, Iliopoulos and Maiani in 1970 [12], known as GIM mechanism, which existence was proved by observation of J/Ψ meson in SLAC [13] and BNL [14]. Formally, GIM allowed a creation of two quark doublets consisting of (u,d) and (s,c). This theory, however, could not lead to CP violation - it was explained by a more general CKM formalism presented in [15].

A way to reproduce the result is to use Yukawa terms L_Y from Standard Model Lagrangian as was presented in [7],

$$L_Y = -Y^d_{ij}\overline{Q^I_{Li}}\phi d^I_{Rj} - Y^u_{ij}\overline{Q^I_{Li}}\varepsilon\phi^* u^I_{Rj} + h.c, \tag{1.8}$$

where Q^I_L stands for left-handed quark doublets, d^I_R and u^I_R for right-handed quark singlets, $Y^{d,u}$ are 3×3 complex matrices, ϕ is a Higgs field generating mass for quarks through spontaneous symmetry breaking, ε - the antisymmetric 2×2 tensor and $i(j) \in 1, 2, 3$ are indices enumerating rows and columns of multiplied tensors. Finally, this is the form in weak interactions eigenbasis. By unitary transformations it can be changed to mass eigenbasis, where $Y^{d,u}$ are diagonalized to the forms of mass matrices $M^{u,d}$,

$$M^{u,d} = V^{u,d}_L Y^{u,d} V^{u,d\dagger}_R (v/\sqrt{2}), \tag{1.9}$$

where $V^{u,d}_{L(R)}$ are basis transformation matrices for left- and right-handed representations respectively and v stands for a scalar field from Higgs field's vacuum expectation value. Considerations can be extended to Weak Interaction terms for charged currents, where transformation matrices act on $W^{+,-}$ gauge fields and the final coupling between left-handed physical quark fields in this basis is not diagonal, but has the form:

$$L_{cc} = \frac{-g}{\sqrt{2}} \begin{pmatrix} \overline{u_L} & \overline{c_L} & \overline{t_L} \end{pmatrix} \gamma^\mu W^+_\mu V_{CKM} \begin{pmatrix} \overline{d_L} \\ \overline{s_L} \\ \overline{b_L} \end{pmatrix} + h.c, \tag{1.10}$$

where γ^μ are the 4×4 Dirac's matrices, g stands for the coupling constant of Weak Interactions and $(u_L, d_L, s_L, c_L, t_L, b_L)$ are the left-handed quark mass states. The new matrix is defined as:

$$V_{CKM} = V^u_L V^{d\dagger}_L = \begin{pmatrix} V_{ud} & V_{us} & V_{ub} \\ V_{cd} & V_{cs} & V_{cb} \\ V_{td} & V_{ts} & V_{tb} \end{pmatrix}. \tag{1.11}$$

It is called the CKM matrix (Cabibbo-Kobayashi-Maskawa) and belongs to SU(3) group. Basically, it mixes quark families between each other, but at a glance it is not apparent how CP violation appears here and a few more steps are needed.

The most general complex 3×3 matrix can be parametrized by 9 moduli and 9 complex phases (due to the exponential form of complex numbers), while the unitarity conditions absorb 6 moduli and 3 phases. At this point, there are still 3 moduli and 6 phases left as free parameters. Another 5 complex phases can be deleted by the redefinition of quark fields by U(1) transformations:

$$q_L \to e^{i\phi_q} q_L, \tag{1.12}$$

where $q_L = u_L, d_L, s_L, c_L, t_L, b_L$. This action leaves the matrix with 3 moduli and 1 complex phase as free parameters, so that the CKM matrix can be decomposed into:

$$V_{\text{CKM}} = \begin{pmatrix} 1 & 0 & 0 \\ 0 & c_{23} & s_{23} \\ 0 & -s_{23} & c_{23} \end{pmatrix} \begin{pmatrix} c_{13} & 0 & s_{13}e^{-i\delta} \\ 0 & 1 & 0 \\ -s_{13}e^{i\delta} & 0 & c_{13} \end{pmatrix} \begin{pmatrix} c_{12} & s_{12} & 0 \\ -s_{12} & c_{12} & 0 \\ 0 & 0 & 1 \end{pmatrix}, \tag{1.13}$$

where $s_{ij} = \sin\theta_{ij}$, $c_{ij} = \cos\theta_{ij}$, θ_{ij} is a mixing angle between i-th and j-th quark family and δ stands for the resting phase. Phase will contribute to a transformed wave function, which is a reason of direct CP symmetry breaking. This theoretical result could explain this effect in kaon decays observed in the experiment described in [10], as it acts in the quark sector. Direct and more appropriate formalism will be defined and discussed extensively in the next subsection.

Measurements of matrix elements were being done in the experiments for last few decades. The most recent result from PDG fit ([7]) is:

$$\begin{aligned} \sin\theta_{12} &= 0.2250 \pm 0.00067, \quad \sin\theta_{13} = 0.00369 \pm 0.00011, \\ \sin\theta_{23} &= 0.04182^{+0.00085}_{-0.00074}, \qquad\quad \delta = 1.144 \pm 0.027. \end{aligned} \tag{1.14}$$

It can be noticed, that mixing between different families have different strengths, so that possible observation of CP violation in quark compounds is connected with the weakening of a probability amplitude by all trigonometric functions. Experimentally, this fact states a serious obstacle, as is directly connected with low branching ratios and makes the requirement for a very careful analysis due to low statistics.

The most important example of CP violation for this thesis are kaons, whose contribution will be explained deeply in the next subsection as well.

1.3 Strange mesons in the context of CPV

Kaons are one of the most iconic examples of complex particles, which were discovered in 1947 in cosmic rays ([16]). Their unexpected behavior, different from other particles known at that time, allowed to state a hypothesis about an existence of strange quark, which became an inevitable supplement to the early theory of quarks created by M. Gell-Mann and independently by G. Zweig. Moreover, it introduced a new quantum number, strangeness, as well.

Group theory approach to find dependencies between particles properties gave a possibility to organize them using a so-called „eightfold way", which through isospin I, hypercharge Y and strangeness S led to nontrivial predictions about particles consisting of quarks. Moreover, SU(3) hypothesis to describe their interactions became a base for the future QCD theory, while the „eightfold way" stays only an approximation.

The topic of the thesis is focused on considerations about neutral kaons, which are produced through strong interactions with $|K^0\rangle$ and $|\overline{K^0}\rangle$ being their eigenstates. Thus, the initial state of kaon is described by the mixture:

$$|K(0)\rangle = a(0)\,|K^0\rangle + b(0)\,|\overline{K^0}\rangle\,, \tag{1.15}$$

where $a(0)$ and $b(0)$ are the initial probability amplitudes for neutral and anti-neutral component, respectively. Moreover, CKM formalism and quark flavor changing show, that kaonic beam will always undergo the equalization of K^0 and $\overline{K^0}$ abundances. This process is called strangeness oscillations and is described by the box diagram visible in Fig. 1, which is a direct implication of quark families mixing.

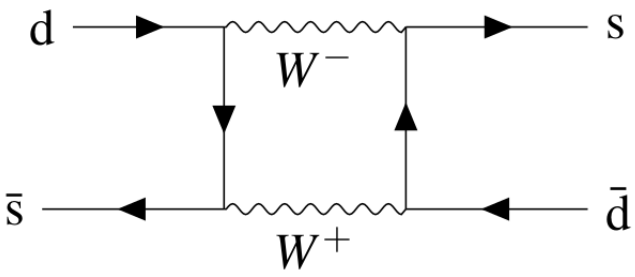

Fig. 1: Box diagram describing strangeness oscillations.

Moreover, kaon propagating in its proper time t can decay into multiple final states. However, due to creation time much shorter than propagation, description of this system can be narrowed down to a subspace of $\{K^0, \overline{K^0}\}$, which is known as Wigner-Weisskopf approximation. Now the total Hamiltonian of the evolution amplitudes can be represented by a Schrödinger equation:

$$i\frac{\partial}{\partial t}\begin{pmatrix} a(t) \\ b(t) \end{pmatrix} = \mathbf{H}\begin{pmatrix} a(t) \\ b(t) \end{pmatrix}, \tag{1.16}$$

where the effective Hamiltonian $\mathbf{H}$ is a complex 2×2 matrix, but due to approximation its hermiticity is lost. It can be decomposed into:

$$\mathbf{H} = \mathbf{M} - \frac{i}{2}\mathbf{\Gamma}, \tag{1.17}$$

where $\mathbf{M}$ stands for an actual mass matrix and $\mathbf{\Gamma}$ for a decay matrix, both hermitian, however, multiplication by $-i/2$ introduces anti-hermiticity to $-\frac{i}{2}\mathbf{\Gamma}$. The connection of this effective expression and the general Hamiltonian of a system, which has the form $\mathcal{H} = \mathcal{H}_0 + \mathcal{H}_{weak}$, is given by the perturbation theory. In this notation $\mathcal{H}_0$ governs EM and strong interactions, while $\mathcal{H}_{weak}$ is responsible for the weak ones, thus, due to the much smaller strength of the weak sector, it can be treated as a perturbation. An actual form of the connection is not needed for further discussion, but can be found in [17].

Generally, $\mathbf{H}$ can be represented in a form:

$$\mathbf{H} = \begin{pmatrix} H_{11} & H_{12} \\ H_{21} & H_{22} \end{pmatrix}, \tag{1.18}$$

where indices 1 and 2 correspond to K^0 and $\overline{K^0}$ respectively. Elements of $\mathbf{H}$ are complex, so in the real domain there are 8 independent parameters - 7 observables and 1 arbitrarily chosen, nonphysical phase. Their concrete configurations give predictions about behavior

of certain symmetries:

$$\begin{aligned} H_{11} \neq H_{22} &\Rightarrow \text{CPT violation}, \\ |H_{12}| \neq |H_{21}| &\Rightarrow \text{T violation}, \\ H_{11} \neq H_{22} \text{ or } H_{11} \neq H_{22} &\Rightarrow \text{CP violation}. \end{aligned} \tag{1.19}$$

To check, however, CP symmetry violation quantitatively a set of appropriate measurable parameters can be established. The first step is a diagonalization of $\mathbf{H}$, giving the eigenvalues:

$$\begin{aligned} \lambda_S &= m_S - i\frac{\Gamma_S}{2}, \\ \lambda_L &= m_L - i\frac{\Gamma_L}{2}, \end{aligned} \tag{1.20}$$

where $m_{S,L}$ and $\Gamma_{S,L}$ are the masses and decay widths of both eigenstates respectively. As these are the stationary states, time evolution multiplies them by a scalar exponential. In fact, they can be noted in a mass basis, i.e. $\{K^0, \overline{K^0}\}$,

$$\begin{aligned} |K_S\rangle &= \frac{1}{\sqrt{2(1+|\varepsilon_S|^2)}} \left[(1+\varepsilon_S)\,|K^0\rangle + (1-\varepsilon_S)\,|\overline{K^0}\rangle \right], \\ |K_L\rangle &= \frac{1}{\sqrt{2(1+|\varepsilon_L|^2)}} \left[(1+\varepsilon_L)\,|K^0\rangle - (1-\varepsilon_L)\,|\overline{K^0}\rangle \right]. \end{aligned} \tag{1.21}$$

This form is especially useful to describe CP symmetry violation, as $\varepsilon_{S,L}$ are small, complex parameters introducing impurities due to this phenomenon. By convention, however, their linear combinations are preferred:

$$\overline{\varepsilon} = \frac{\varepsilon_S + \varepsilon_L}{2},\ \delta = \frac{\varepsilon_S - \varepsilon_L}{2}, \tag{1.22}$$

and moreover they can be represented by $\mathbf{H}$ elements in a way:

$$\begin{aligned} \overline{\varepsilon} &= \frac{H_{12} - H_{21}}{2(\lambda_S - \lambda_L)}, \\ \delta &= \frac{H_{11} - H_{22}}{2(\lambda_S - \lambda_L)}. \end{aligned} \tag{1.23}$$

Off-diagonal terms of $\mathbf{H}$ are phase dependent, so $\overline{\varepsilon}$ is not defined uniquely.

Before the measurements, a certain convention of phase value has to be adapted. After some manipulations, included in [17], it can be found, that:

$$4\Re\overline{\varepsilon} \approx \frac{|H_{12}|^2 - |H_{21}|^2}{|H_{12}|^2 + |H_{21}|^2}, \tag{1.24}$$

where phase independence makes it a physical quantity. Finally, experimentally useful relations can be stated basing on derived parameters:

$$\begin{aligned} \delta \neq 0 &\Rightarrow \text{CPT violation}, \\ \Re\overline{\varepsilon} \neq 0 &\Rightarrow \text{T violation}, \\ \Re\overline{\varepsilon} \neq 0 \text{ or } \delta \neq 0 &\Rightarrow \text{CP violation}. \end{aligned} \tag{1.25}$$

Additionally, $\mathbf{H}$ can be parametrized with 7 observables: 4 in complex eigenvalues $\lambda_{S,L}$, 2 in the complex parameter δ and 1 as the real part of $\overline{\varepsilon}$.

Moreover, another phenomenon having an impact on further analysis can be described for strange mesons. *Regeneration effect* is caused by K_L interacting with the atoms of the material it flies through. K_L then has a non-zero probability to become a K_S. The first observation is described in [18].

1.4 Decays of correlated kaons

For the purposes of this thesis, a system of correlated kaons has to be explained. It appears, that kaon pairs can be produced in strong decays of light, unflavored mesons, especially $\phi(s\overline{s})$ characterized with (data taken from [7]) $J^{PC} = 1^{--}$, $S = 0$, a mass:

$$m_\phi = (1019.461 \pm 0.016)\ \mathrm{MeV/c^2}, \tag{1.26}$$

and:

$$BR(\phi \to K_S K_L) = (33.9 \pm 0.4)\%. \tag{1.27}$$

Properties of ϕ meson actually narrow down the possibilities of produced kaons to two cases:

$$\begin{aligned} &|K^0(+\mathbf{p})\rangle\, |\overline{K^0}(-\mathbf{p})\rangle\,, \\ &|\overline{K^0}(+\mathbf{p})\rangle\, |K^0(-\mathbf{p})\rangle\,, \end{aligned} \tag{1.28}$$

where momentum $\mathbf{p}$ is in CM frame of ϕ. It can be shown, however, that an initial state of propagation coming from the decay of vector mesons is ([17]):

$$|i\rangle = \frac{N}{\sqrt{2}} \left[|K_S(+\mathbf{p})\rangle\, |K_L(-\mathbf{p})\rangle - |K_L(+\mathbf{p})\rangle\, |K_S(-\mathbf{p})\rangle \right], \tag{1.29}$$

with the normalization constant:

$$N = \frac{\sqrt{(1+|\varepsilon_S|^2)(1+|\varepsilon_L|^2)}}{1-\varepsilon_S\varepsilon_L}. \tag{1.30}$$

The probability amplitude of the decay into final states f_1 and f_2 can be calculated using standard rules of quantum mechanics. Firstly, the initial state is transformed using

continuous time evolution and finally the amplitude is determined as:

$$A(f_1,t_1;f_2,t_2) = \frac{N}{\sqrt{2}}\Big[\langle f_1|\hat{S}|K_S\rangle\langle f_2|\hat{S}|K_L\rangle e^{-i\lambda_S t_1}e^{-i\lambda_L t_2} - \langle f_1|\hat{S}|K_L\rangle\langle f_2|\hat{S}|K_S\rangle e^{-i\lambda_L t_1}e^{-i\lambda_S t_2}\Big], \tag{1.31}$$

where $t_{1(2)}$ indicate the proper time of a given kaon and $\hat{S}$ - a scattering matrix. According to [17], the double differential decay rate integrated over t_1+t_2 for Eq. (1.31) in the function of $\Delta t = t_2 - t_1$ is:

$$I(f_1,f_2;\Delta t) = \frac{C_{12}}{\Gamma_S+\Gamma_L}\Big[|\eta_1|^2 e^{-\Gamma_L\Delta t} + |\eta_2|^2 e^{-\Gamma_S\Delta t} - 2|\eta_1||\eta_2|e^{-\frac{\Gamma_S+\Gamma_L}{2}\Delta t}\cos\left[\Delta m\Delta t + \phi_2 - \phi_1\right]\Big], \tag{1.32}$$

valid for $\Delta t \geq 0$, while for $\Delta t < 0$ substitutions $\Delta t \to |\Delta t|$ and $1 \rightleftarrows 2$ have to be applied. The parameters are equal to:

$$\eta_i = |\eta_i|e^{i\phi_i} = \frac{\langle f_i|\hat{S}|K_L\rangle}{\langle f_i|\hat{S}|K_S\rangle}, \qquad C_{12} = \frac{|N|^2}{2}|\langle f_1|\hat{S}|K_S\rangle\langle f_2|\hat{S}|K_L\rangle|^2. \tag{1.33}$$

In Eq. (1.32) a term proportional to trigonometric contribution is called an *interference term*, which leads to the characteristic correlation between two kaon decays. The mathematical form of the *interference function* is, however, arbitrary on the level of parametrization. For the special case of $K_S K_L \to \pi^+\pi^-\pi^0\pi^0$ decay analyzed in these studies, the conventionally used parameter to measure the level of direct CP symmetry violation is ε'/ε. This type of breaking is interpreted as the direct decays of CP-even states into CP-odd ones and vice versa, which should be forbidden. For the completeness, the indirect one ($\overline{\varepsilon} \neq 0$ is tied with the non-existence of a common eigenbasis of **H** and CP operators, so it has to occur every time, if the linear algebra is correct. Connection of ε'/ε with η_i is given by:

$$\eta_{+-} = |\eta_{+-}|e^{i\phi_{+-}} = \varepsilon + \varepsilon', \qquad \eta_{00} = |\eta_{00}|e^{i\phi_{00}} = \varepsilon - 2\varepsilon', \tag{1.34}$$

and using it Eq. (1.32) can be transformed in a more suitable form for CP violation measurement in KLOE experiment, which is:

$$\begin{aligned} &I(f_1, f_2; \Delta t \geq 0) = \\ &C_{12}\frac{|\varepsilon|^2}{\Gamma_S + \Gamma_L}\Big[(1 + 2\mathrm{Re}(\varepsilon'/\varepsilon))e^{-\Gamma_L \Delta t} + (1 - 4\mathrm{Re}(\varepsilon'/\varepsilon))e^{-\Gamma_S \Delta t} \\ &-2e^{-\frac{\Gamma_S+\Gamma_L}{2}\Delta t}((1 - \mathrm{Re}(\varepsilon'/\varepsilon))\cos(\Delta m \Delta t) + 3\mathrm{Im}(\varepsilon'/\varepsilon)\sin(\Delta m \Delta t))\Big]. \end{aligned} \tag{1.35}$$

depending explicitly on ε'/ε - derivation is available in Appendix A. Level of symmetry violation is connected with these parameters and is visible through the shape of a graph shown in Fig. 2. Interference can be noticed around $\Delta t = 0$, where $\tau_S = (8.954 \pm 0.004) \cdot 10^{-2}$ ns is a mean lifetime of K_S. Number of events drops exactly in the center and then, around $|\Delta t| \sim 5\ \tau_S$, reaches maximal values.

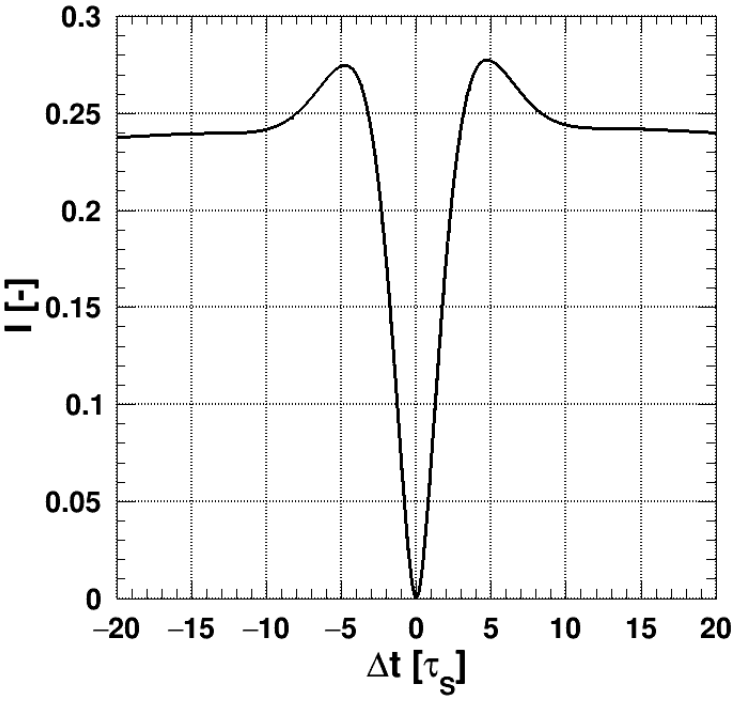

Fig. 2: Graph of Eq. (1.35) with recent parameters from [7] equal to $\mathrm{Re}(\varepsilon'/\varepsilon) = 1.66 \cdot 10^{-3}$ and $\mathrm{Im}(\varepsilon'/\varepsilon) = -1.97 \cdot 10^{-3}$. Due to non-zero $\mathrm{Im}(\varepsilon'/\varepsilon)$ the maxima around $|\Delta t| \sim 5\ \tau_S$ are not symmetric.

The actual asymmetry of peaks is connected with a non-zero $\mathrm{Im}(\varepsilon'/\varepsilon)$, so could indicate, as will be discussed later, the violation of CPT symmetry. Finally, all of the branching ratios for the considered decays are shown in Table 1. Thus, jointly with Eq. (1.27), the total event's branching ratio is equal to:

$$BR(\phi \to K_S K_L \to \pi^+\pi^-\pi^0\pi^0) \approx 0.04\%, \tag{1.36}$$

which shows how precise should be the measurements of CP violation in strange mesons' systems.

Decay channel	Value [%]	Error [%]
$BR[K_S \to \pi^0\pi^0]$	30.69	0.05
$BR[K_S \to \pi^+\pi^-]$	69.20	0.05
$BR[K_L \to \pi^0\pi^0]$	0.0864	0.0002
$BR[K_L \to \pi^+\pi^-]$	0.197	0.001

Table 1: Branching ratios of the considered decays. Details can be found in [7].

1.5 Experimental results in the field

As was said before, CP violation in neutral mesons systems stays under a constant study for last over 60 years. Due to its long history, it is important to build a base of results and approaches used before to compare with final results. Here only the experiments taken for the average and fit of $\mathrm{Re}(\varepsilon'/\varepsilon)$ and $\mathrm{Im}(\varepsilon'/\varepsilon)$ by PDG are taken into account. Values of mentioned parameters are collected in Table 2.

$\mathrm{Re}(\varepsilon'/\varepsilon) \times 10^{-3}$	$\mathrm{Im}(\varepsilon'/\varepsilon) \times 10^{-3}$	Collaboration
$0.74 \pm 0.52 \pm 0.29$	–	E731 [19]
2.30 ± 0.65	–	NA31 [20]
1.47 ± 0.22	–	NA48 [21]
1.92 ± 0.21	-1.72 ± 2.02 (not assuming CPT)	kTeV [22]
1.68 ± 0.20	–	PDG average [7]
1.66 ± 0.23	-1.92 ± 1.92 (not assuming CPT)	PDG fit [7]

Table 2: Results of previous experiments taken for PDG average and fit. PDG fitted values will be used in all calculations.

$\mathrm{Re}(\varepsilon'/\varepsilon)$ and $\mathrm{Im}(\varepsilon'/\varepsilon)$ determined in kTeV was actually a result of second analysis, first one is available in [23], but used only half of the available collected data. PDG fit, being a combined result, took into account both $\mathrm{Re}(\varepsilon'/\varepsilon)$ and $\mathrm{Im}(\varepsilon'/\varepsilon)$, so it will be used as the reference point of a whole analysis.

Most of the previous approaches were based on the collision of hadrons accelerated in the attached collider with a static target. There, through strong interactions, a beam of kaons and anti-kaons was produced, but a propagation extending over τ_S left it in the state of a pure K_L beam. K_S therefore was produced through regeneration on another target,

so that products of two beams, one consisting of K_S and one of K_L, were registered in the detectors. In this context KLOE can be described as a novel approach to this topic, where regeneration is treated as a background, rather than a source of measured quantities. It is believed to be a more convenient approach, as regeneration is in fact a complicated process, which could introduce subtle, unforeseen impact on the final result. Absolute uncertainties of $\mathrm{Re}(\varepsilon'/\varepsilon)$ for all the experiments stay at the order of, 10^{-4} and KLOE was designed to reach such level of precision ([24]). Predicted value of $\mathrm{Re}(\varepsilon'/\varepsilon)$ minimal statistical uncertainties basing on MC-MC fit (described extensively in [1]) can be seen in Fig. 3.

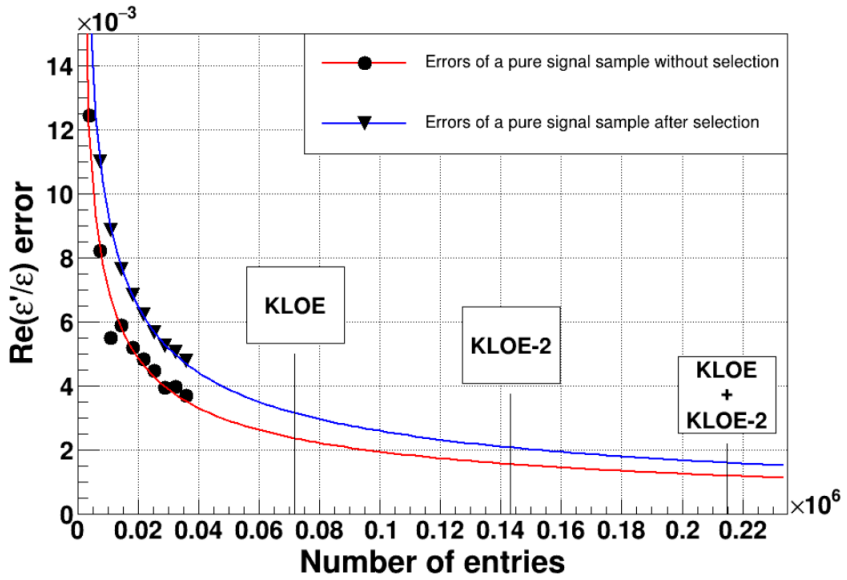

Fig. 3: Prediction of minimal uncertainties of $\mathrm{Re}(\varepsilon'/\varepsilon)$ determination. Analysis was done on Monte Carlo reconstructed events, so determination of errors without selection used the total sample before cut analysis, while after selection - with cuts imposing signal hypothesis. Plot adapted from [1].

It can be seen, that all the experiments, besides kTeV collaboration, did not determine $\mathrm{Im}(\varepsilon'/\varepsilon)$ at all. Instead, CPT symmetry was qualified as a fundamentally conserved symmetry during the analyses, which implicated $\mathrm{Im}(\varepsilon'/\varepsilon) = 0$. KTeV experiment, however, decided to lead two analyses, one assuming CPT symmetry conservation and the other without this premise. This constituted the first measurement of $\mathrm{Im}(\varepsilon'/\varepsilon)$ parameter, but its precision stays at the level of 100% relative uncertainty. Using the interference function in KLOE it is a natural step to fit it leaving $\mathrm{Im}(\varepsilon'/\varepsilon)$ as a free parameter giving a possibility to study CP violation fully, which makes it a first approach to determine both parameters at once. Similar plot as before, involving absolute uncertainty of $\mathrm{Im}(\varepsilon'/\varepsilon)$ visible in Fig. 4.

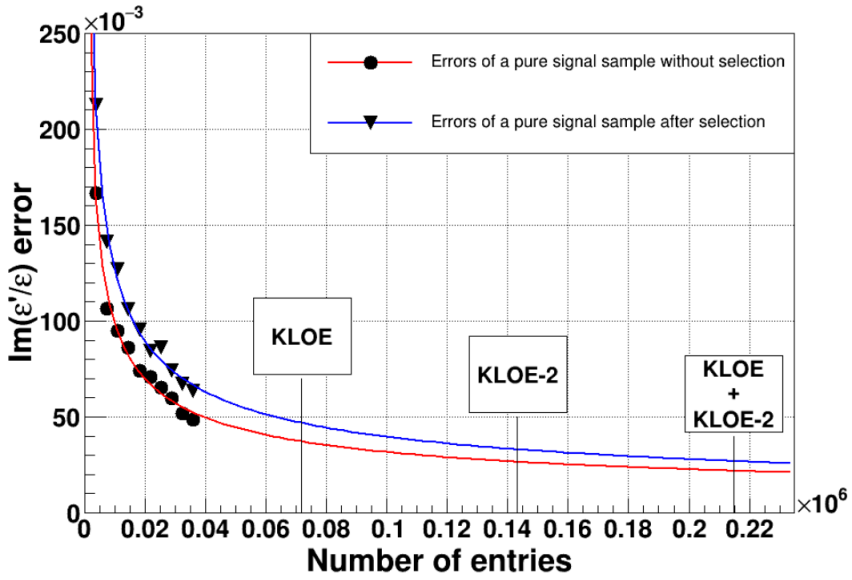

Fig. 4: Prediction of minimal uncertainties of $\mathrm{Im}(\varepsilon'/\varepsilon)$ determination. Analysis was done on Monte Carlo reconstructed events, so determination of errors without selection used the total sample before cut analysis, while after selection - with cuts imposing signal hypothesis. Plot adapted from [1].

2 Experimental setup

Before getting into the details on the analysis, it is worth to mention the structure of a used experimental setup. This section will be divided into three parts describing the DAΦNE e^+e^- collider, KLOE detector used in 2005-2006 operation and upgrades made for 2014-2018 data collection.

2.1 DAΦNE accelerator

Titular electron-positron collider is placed in Laboratori Nazionali di Frascati INFN and belongs to the separate class of synchrotrons named Φ-factories. A scheme of the complex with detailed naming of system's elements is visible in Fig. 5. An electron beam up to 10 A with 120 keV average energy is initially delivered from triode gun to the LINAC and after ~ 3 m of an accelerating section is focused by the magnetic quadrupoles to hit the static target and produce positrons with an efficiency $\sim 0.9\%$ ([26]). Positrons are collected by electromagnets, the second beam is formed and accelerated up to 550 MeV. At the same time, the e^- beam reaches the energy of around 800 MeV and finally both enter the accumulator, which is the intermediate step before the injection into the main rings. The energy of each beam is adjusted to ~ 510 MeV, which states the most optimal situation for ϕ meson production in CM frame for two opposing beams it corresponds to ϕ meson's mass. Finally, beams are injected into the actual DAΦNE rings, where the collision was allowed in the interaction region inside the KLOE detector with the crossing angle of

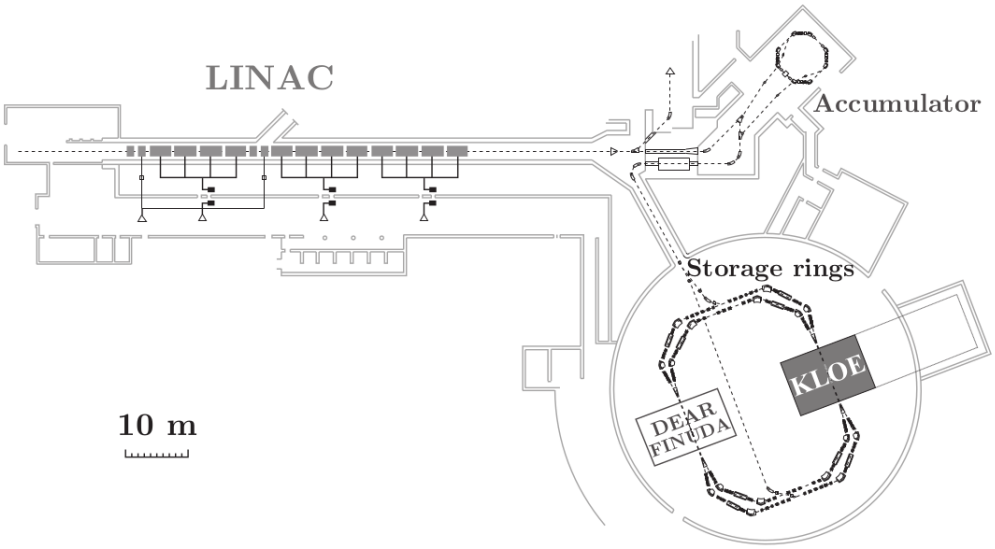

Fig. 5: Complex of Φ-factory with detailed elements. The system is adjusted to $\sqrt{s} \approx 1020$ MeV corresponding to the mass of ϕ meson. Scheme available in [25].

25 mrad. According to Eq. (1.27) production of ϕ meson gives an actual opportunity to study correlated kaons and possible CP violating events.

More technical details of the accelerator complex along with the documentation can be found on webpage in [26].

2.2 KLOE detector

The main tool used for the measurements was KLOE detector, which had a multi-layer construction visible in Fig. 6 revealing the y-z plane. For the completeness, z-axis is parallel to the beam pipe, x-axis is perpendicular to it and horizontal, while y-axis is vertical. KLOE can be divided in two main parts: drift chamber (DC) and electromagnetic calorimeter (EMC). Due to the requirement of Δt measurement being at the order of τ_S, innovative solutions were applied to reach needed resolutions to resolve a structure near $\Delta t = 0$. The properties of each element will be described in the following paragraphs.

2.2.1 Interaction Point (IP)

$K_S K_L$ pairs are produced in the IP (close to the geometrical center of a detector), but to reach the drift region one has to pass the beam pipe and the inner wall of DC, mostly K_L due to long mean decay length of ∼340 cm (in [7]). Exactly here importance have the regeneration. Formally, for KLOE it gives $K_S K_L \to K_S K_S \to \pi^+\pi^-\pi^0\pi^0$ decay, so although the products are the same as expected, there is no CP violation engaged. Finally, it constitutes one of the background components for the further analysis and has to be minimized by the construction of a beam pipe and DC themselves.

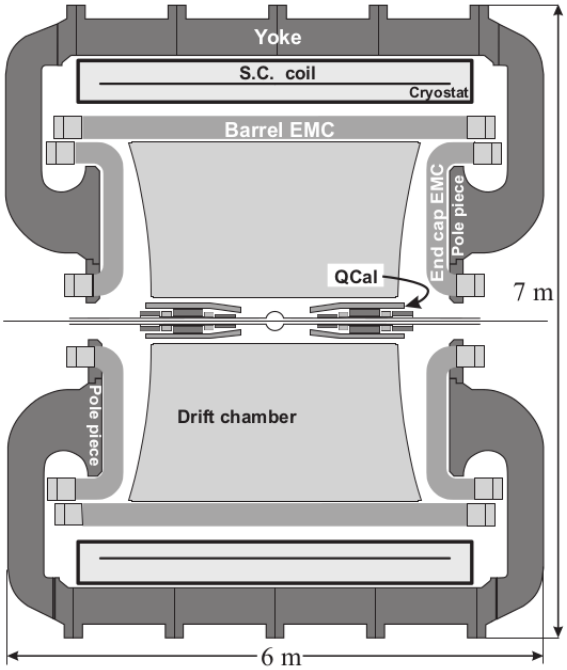

Fig. 6: Scheme of KLOE detector with denoted dimensions and the components on y-z plane. Image adapted from [25]

Beam pipe, visible in Fig. 7, of a 10 cm radius centered at IP has a thickness $500\ \mu\mathrm{m}$ and is made out of 62% beryllium and 38% aluminum alloy. Regeneration strongly depends on the distance flown in the material, so the shape of a beam pipe around IP is spherical to minimize it. These properties reduce the impact of regeneration and, moreover, decay length of K_S ($\sim$0.6 cm) ensures, that it stays inside the spherical region. As was mentioned before, regeneration can occur at the inner wall of DC [27], as well it is placed at the radius 25 cm from the IP and has layers of $750\ \mu\mathrm{m}$ thick carbon fiber and $150\ \mu\mathrm{m}$ thick aluminum.

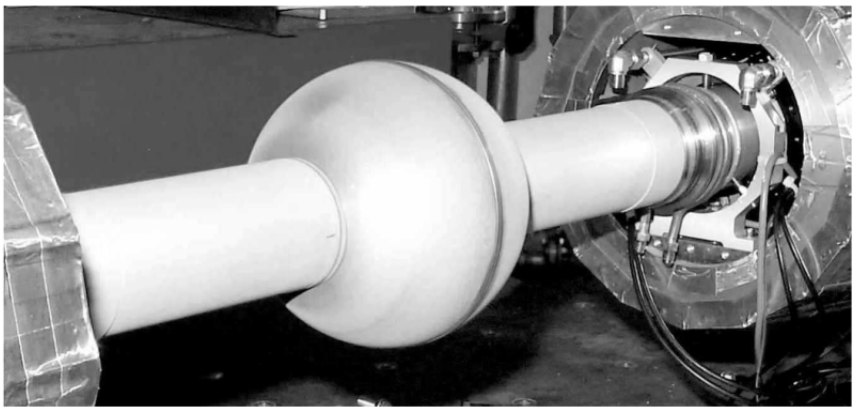

Fig. 7: Construction of a spherical beam pipe around IP. Image adapted from [28].

2.2.2 Drift chamber

It is a main part of the system, allowing the precise measurement of vertex position and momenta of charged products of kaon decays. Geometrically, it has a shape of a cylinder with 4 m diameter and 3.3 m length, which were chosen due to the mentioned large mean decay length of K_L. Moreover, due to EMC being at the boundary, DC has to be transparent to all neutral particles to let them reach the calorimeter.

The principle of operation is based on the ionization of gas filling the chamber by charged particles passing through the region. Actually, a gaseous mixture of 90% helium and 10% isobutane playing a role of quencher is the active fulfillment. After a primary ionization, due to the strong electric field close to the wires, an ionization cascade has place and after approaching the wire a signal is detected. Position of a pass is given by a time difference between signals in different wires, i.e., length from track to each wire can be calculated. To provide a very good resolution of track reconstruction, KLOE use $\sim$52000 wires. Cells allowing measurement on x-y plane are visible in Fig. 8, while for z-coordinate a mutual twist of wires was applied.

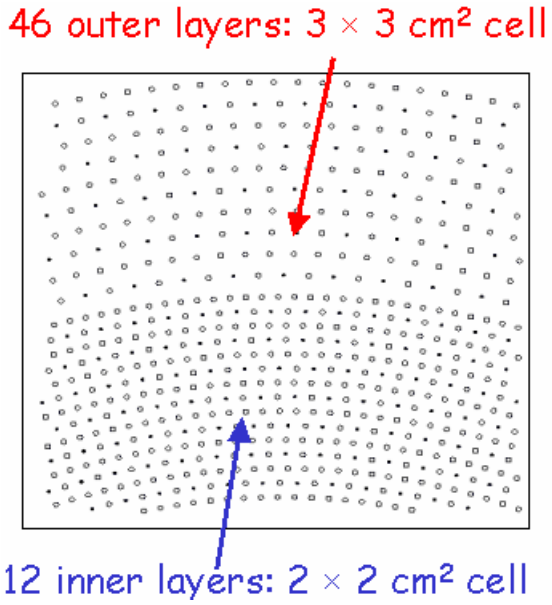

Fig. 8: Arrangement of x-y plane wire cells in the DC. Image adapted from [29].

To determine particles' momenta, DC is placed inside a uniform magnetic field of $\sim$0.52 T directed along z axis and causing bending of trajectories due to Lorentz's Force. Basic quantities, due to cylindrical shape of DC, are R_T (transverse radius), φ (azimuthal angle), θ (polar angle), which give compact formulas for momentum:

$$\begin{aligned} p_x &= qBR_T \cos(\varphi), \\ p_y &= qBR_T \sin(\varphi), \\ p_z &= qBR_T \cot(\theta), \end{aligned} \tag{2.1}$$

and as can be seen, x-y momentum value depends only on charge of particle q and magnetic field B. KLOE DC allows measuring momenta with a relative resolution at the order of $\sim 0.3\%$. Vertex of origin of charged tracks is found using a tracking algorithm. It is based on the determination of point of intersection of extrapolated tracks details are available in [30].

Finally, it is worth mentioning, that KLOE DC was a state-of-the-art being the biggest drift chamber in the world at the time of construction as well as at the moment of decommissioning. More information and details about calibration can be found in [27].

2.2.3 Electromagnetic calorimeter

It is third and the outermost element. Kinematics of neutral particles passing the DC is not perturbed due to its high transparency. The task of EMC is, thus, to absorb them and measure their energy with the resolution as good as possible. Most importantly, however, as CPV events partially consist of $K_L \to \pi^0\pi^0 \to 4\gamma$ decays, EMC can detect localization of absorbed photons and using them reconstruction of the vertex and finally time of flight of K_L is possible. The excellent time resolution of EMC is at the order of interference function scale, so it gives a possibility to measure CP violation using $\mathrm{K_S K_L} \to \pi^+\pi^-\pi^0\pi^0$. An overview of EMC composed with $\mathrm{K_S K_L} \to \pi^+\pi^-\pi^0\pi^0$ event is visible in Fig. 9.

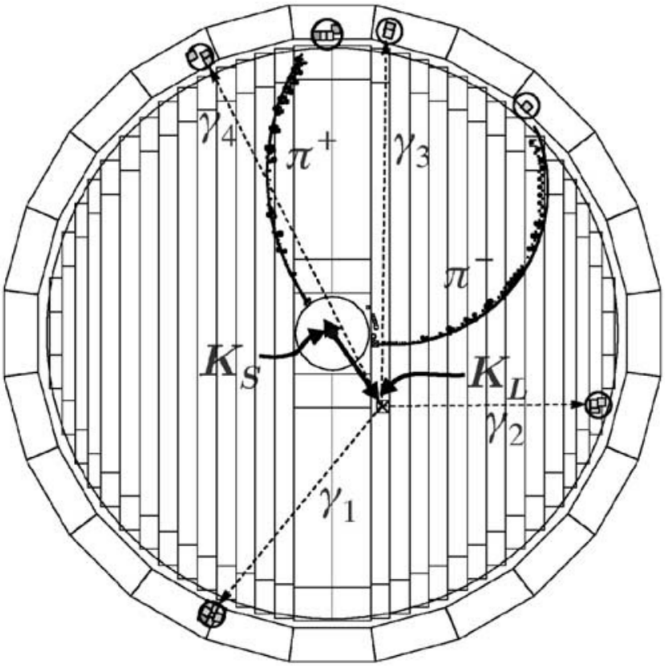

Fig. 9: x-y plane projection of EMC with a visible end cap in front and a barrel-shaped part surrounding it. Image adapted from [24].

EMC consists of two main parts: 4.3 m long cylindrical barrel parallel to z axis made from trapezoidal blocks of scintillating fibers submerged in epoxy between 0.5 mm thick lead foils and two end caps of a rectangular cross-section covering x-y plane both visible

in Fig. 6. Their overlap creates almost 4π detector with an only dead part around the beam pipe to register these particles, QCAL detector was included (not used in the analysis of this thesis). Collection of secondary photons was realized using light guides, for which the measured efficiency was better than 80 %, ending with photomultipliers. To protect them from the impact of the magnetic field, cavities in pole pieces were placed reducing the component transverse to photomultipliers to about 0.07 T. [24]

Reconstruction of photon showers starts with a clustering algorithm determining, which fibers were activated by the same particle entering the active region. Resolution of a read-out in x-z plane gives $\sim$1.3 cm, which corresponds to the shower size [24]. Energy resolution was determined by the use of minimum ionizing particles and EM showers, while calorimeter timing was calibrated using cosmic rays and radiative events (Bhabha scattering, 2γ and ϕ decays). Final resolutions for both energy and time used in the further analysis are [24, 29]:

$$\sigma_E/E = 5.7\%/\sqrt{E(\mathrm{GeV})},\ \sigma_t = 54\ \mathrm{ps}/\sqrt{E(\mathrm{GeV})} \oplus 50\ \mathrm{ps}, \tag{2.2}$$

and high efficiency of energy reconstruction is set to be above 20 MeV for a cluster.

More technical details, a specified description of electronics used in a read-out and measurements of resolutions are available in [24, 29].

2.3 KLOE-2 upgrades

KLOE experiment worked in two stages, 2001-2002 and 2004-2005, when it collected a total integrated luminosity of 2.5 fb^{-1}. A second experiment, however, was planned to reach even higher luminosity to increase statistics and improve the detector. KLOE-2 collaboration was collecting the DATA in a term 2014-2018 and got the luminosity of 5 fb^{-1}. The detector was enriched with a gas-electron multiplier part ([31]) placed between the spherical beam pipe and the inner wall of the DC and playing the role of an Inner Tracker. IT had the task to register decays close to IP and include them in the analysis, which was not possible in KLOE. Moreover, an improved QCAL detector ([32]) was developed to register particles directed in the dead angle of a beam pipe, along with new crystal ones (CCALT) described in [33]. KLOE-2 DATA are not used in the analysis of this thesis, description was included for the completeness.

3 Measurement principle

Before the actual analysis, an idea of a measurement and all assumptions taken for the selection of channels and determination of the final quantity have to be established. In this section the control samples definition will be given along with a general outline of

an algorithm for their selection. Moreover, the significant differences between efficiency determined from Monte Carlo and from collected DATA will be a foundation of the determination of a correction factor, which will be used to improve the final result of $\mathrm{Re}(\varepsilon'/\varepsilon)$ and $\mathrm{Im}(\varepsilon'/\varepsilon)$.

3.1 Significance of control samples in the context of CPV studies

Measurements of CP violation in $\mathrm{K_S K_L} \to \pi^+\pi^-\pi^0\pi^0$ channel need an increased precision due to very low abundance of such events in the collected Data vide Table 1. Actually, measurement path can be divided into a few steps:

1. Reconstruction of physical quantities using initially filtered events.
2. Selection under the hypothesis of $\mathrm{K_S K_L} \to \pi^+\pi^-\pi^0\pi^0$ channel step fulfilled in [1].
3. Subtraction of resting background from the resulting spectra.
4. Correction of the obtained distribution by $\mathrm{K_S K_L} \to \pi^+\pi^-\pi^0\pi^0$ selection efficiency $\epsilon(\Delta t)$ to get the *expected* signal's spectrum.
5. Fit of Eq. (5.10) by minimizing χ^2 between Δt distributions first one obtained from DATA and second one being reconstructed MC, which is weighted with mentioned Eq. (5.10) (method described in details in [1])
6. Determination of uncertainties and values of $\mathrm{Re}(\varepsilon'/\varepsilon)$ and $\mathrm{Im}(\varepsilon'/\varepsilon)$.

This thesis focuses on the proper determination of efficiency to get the most reliable result of $\mathrm{Re}(\varepsilon'/\varepsilon)$ and $\mathrm{Im}(\varepsilon'/\varepsilon)$ in the end of the analysis.

In this context, efficiency is defined in the function of Δt by:

$$\epsilon(\Delta t)_i = \frac{N_i^{\mathrm{sel}}}{N_i^{\mathrm{tot}}}, \tag{3.1}$$

where $i = \{K \to \pi^+\pi^-,\ K \to \pi^0\pi^0\}$ enumerates the channel and sel (tot) indicates a number of selected (total) events for i-th channel, respectively. By default, to avoid additional indices, every $\epsilon(\Delta t)_i$, N_i^{sel} and N_i^{tot} is actually calculated for the given bin of Δt distribution. To determine it one can directly use Monte Carlo (will be further used as $\epsilon(\Delta t)_i^{\mathrm{MC}}$) as it fully describes predicted channels and effects with luminosities known from the actual measurements and with respect to the knowledge available at the moment of its creation. The very last part constitutes the most serious flaw of this approach - possible impact of earlier wrong expectations on the current measurement.

For the special case of KLOE experiment, however, it is possible to fix it using DATA, which brings the actual physical information about the numbers of events. Practically, $\mathrm{K_S K_L} \to \pi^+\pi^-\pi^0\pi^0$ consists of two differently reconstructed parts: $K \to \pi^+\pi^-$ and the

ones decaying into $K \to \pi^0\pi^0$. Thus, two separate situations have to be considered - they are visible in Fig. 10.

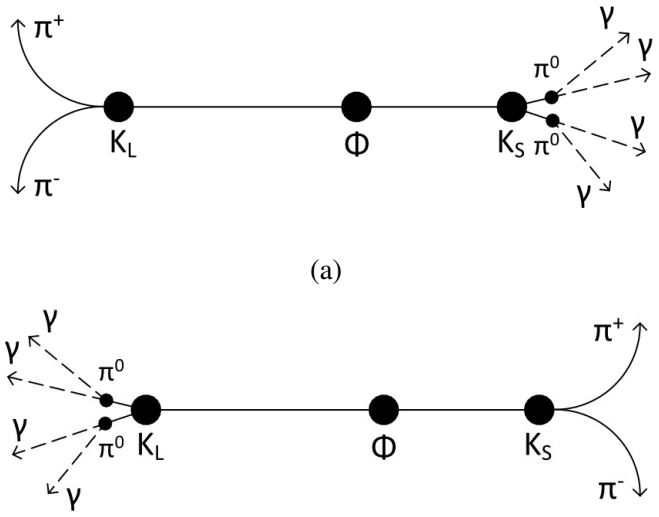

(a)

(b)

Fig. 10: Visualization of two possible signal events. In the analysis, identical decays of $\mathrm{K_S}$ and $\mathrm{K_L}$ are mixed, but separation is needed to choose control samples, which will be used to fix MC efficiency.

Worth mentioning is the fact, that there is no assignment of K to $\mathrm{K_S}$ and $\mathrm{K_L}$ - due to Table 1 they should be mixed in both charged and neutral decays. The main goal is to find *correction factor* from DATA to both charged and neutral parts, but using so-called *control samples*. The corrected efficiency then is defined as:

$$\epsilon(\Delta t)^{\mathrm{corr}} = f(\Delta t) \times \epsilon(\Delta t)^{\mathrm{MC}}, \tag{3.2}$$

where $f(\Delta t)$ is a correction factor - will be defined in more detail in next subsection. Such an approach is based on an assumption, that decays' probabilities of $\mathrm{K} \to \pi^+\pi^-$ are totally independent of $\mathrm{K} \to \pi^0\pi^0$, thus mathematically their branching ratios are multiplicative and allow constituting a single factor.

Control samples mentioned earlier are subsamples of available DATA, which can be used to calculate a correction factor independently of $\mathrm{K_S K_L} \to \pi^+\pi^-\pi^0\pi^0$ events. The actual three decay channels were chosen and are listed in Table 3 along with their branching ratios.

As can be seen, $\mathrm{K_S K_L} \to \pi^+\pi^-3\pi^0$ provides only $\mathrm{K_S} \to \pi^+\pi^-$, but is abundant in DATA. To get $\mathrm{K_L} \to \pi^+\pi^-$, a CPV violating channel $\mathrm{K_S K_L} \to \pi^+\pi^-\pi^+\pi^-$ is chosen as well. Moreover, $\mathrm{K_S K_L} \to \pi^\pm \mathrm{l}^\mp \nu \pi^0\pi^0$ fulfills $\mathrm{K_S}$ and $\mathrm{K_L}$ decays simultaneously. Finally, they are being selected using a following algorithm:

Decay channel	BR [%]	Tagging part	Signal-like part
$\mathrm{K_S K_L} \to \pi^{\pm} l^{\mp} \nu \pi^0 \pi^0$	20.74	$K \to \pi^{\pm} l^{\mp} \nu$	$K \to \pi^0 \pi^0$
$\mathrm{K_S K_L} \to \pi^+ \pi^- 3\pi^0$	13.51	$K_L \to \pi^0 \pi^0 \pi^0$	$K_S \to \pi^+ \pi^-$ [1]
$\mathrm{K_S K_L} \to \pi^+ \pi^- \pi^+ \pi^-$	0.14	$K \to \pi^+ \pi^-$	$K \to \pi^+ \pi^-$ [2]

Table 3: Chosen decay channels used for the determination of control samples.

1. Choice of channel in which one decay branch is identical to signal's.
2. Independent reconstruction of both charged and neutral branches to avoid their mutual correlations
3. Selection of a chosen channel basing on kinematics constraints and topology of an event, *but* imposing cuts only on the tagging part.
4. Imposing selection under signal hypothesis on the signal-like part basing on [1].

The independence of reconstruction between two decay branches is crucial - it removes correlations, so finally an obtained signal-like sample does not depend on cuts of a tagging part and can serve as the estimation of $\mathrm{K_S K_L} \to \pi^+ \pi^- \pi^0 \pi^0$ events. Having the algorithm fulfilled, it is possible to calculate correction factor.

3.2 Correction factor determination method

Before approaching the correction factor $f(\Delta t)$, the properties of general efficiency calculation have to be established. Starting with a case of Monte Carlo events, the formulas for both decays of kaons can be written explicitly as:

$$\begin{aligned} \epsilon(\Delta t)^{\mathrm{MC}}_{\mathrm{K}\to\pi^+\pi^-} &= \frac{N^{\mathrm{sel}}_{\mathrm{K}\to\pi^+\pi^-}}{N^{\mathrm{tot}}_{\mathrm{K}\to\pi^+\pi^-}}, \\ \epsilon(\Delta t)^{\mathrm{MC}}_{\mathrm{K}\to\pi^0\pi^0} &= \frac{N^{\mathrm{sel}}_{\mathrm{K}\to\pi^0\pi^0}}{N^{\mathrm{tot}}_{\mathrm{K}\to\pi^0\pi^0}}, \end{aligned} \tag{3.3}$$

and if these selections were performed independently and decays are not correlated, the total efficiency for $\mathrm{K_S K_L} \to \pi^+ \pi^- \pi^0 \pi^0$ can be calculated as a multiplication. This is not the case for the direct $\mathrm{K_S K_L} \to \pi^+ \pi^- \pi^0 \pi^0$ selection, because the reconstruction method of neutral vertex (i.e., $K \to \pi^0 \pi^0$) uses direction and magnitude of $K \to \pi^+ \pi^-$ momentum,

[1] Decay close from IP
[2] Decay far from IP

so introduces dependence between both vertices (method described in details in Appendix BAppendix B). Thus, the final formula for $\epsilon(\Delta t)^{\mathrm{MC}}_{\mathrm{K_S K_L}\to\pi^+\pi^-\pi^0\pi^0}$ is:

$$\epsilon(\Delta t)^{\mathrm{MC}}_{\mathrm{K_S K_L}\to\pi^+\pi^-\pi^0\pi^0} = \frac{N^{\mathrm{sel}}_{\mathrm{K_S K_L}\to\pi^+\pi^-\pi^0\pi^0}}{N^{\mathrm{tot}}_{\mathrm{K_S K_L}\to\pi^+\pi^-\pi^0\pi^0}}. \tag{3.4}$$

Approach with the independent selection, however, has an application for control samples. As was mentioned in the previous subsection, after selection of a control sample channel, the signal selection for $\mathrm{K}\to\pi^+\pi^-$ or $\mathrm{K}\to\pi^0\pi^0$ is imposed on it. To make it clear, the algorithms for both signal-like parts are described explicitly in Table 4 and Table 5. It has to be denoted, that $N^{\mathrm{tag}}_{\mathrm{K}\to\pi^0\pi^0}$ consists of two possible combinations of decays: $\mathrm{K_S}\pi^\pm l^\mp\nu$ and $\mathrm{K_L}\pi^0\pi^0$ or the other way around, similarly for $N^{\mathrm{tag}}_{\mathrm{K}\to\pi^+\pi^-}$. Due to this fact, the proportions of both tagging decays have to be estimated to properly assign branching ratios for expected decays - they are called p_i, where $i = 1, 2, 3, 4$, and are equal to:

$$\begin{aligned}
p_1 &= \frac{BR[\mathrm{K_S}\to\pi^\pm l^\mp\nu]}{BR[\mathrm{K_S}\to\pi^\pm l^\mp\nu] + BR[\mathrm{K_L}\to\pi^\pm l^\mp\nu]} \approx 0.18\%,\\
p_2 &= \frac{BR[\mathrm{K_L}\to\pi^\pm l^\mp\nu]}{BR[\mathrm{K_S}\to\pi^\pm l^\mp\nu] + BR[\mathrm{K_L}\to\pi^\pm l^\mp\nu]} \approx 99.82\%,\\
p_3 &= \frac{BR[\mathrm{K_S}\to\pi^+\pi^-]}{BR[\mathrm{K_S}\to\pi^+\pi^-] + BR[\mathrm{K_L}\to\pi^+\pi^-]} \approx 99.72\%,\\
p_4 &= \frac{BR[\mathrm{K_L}\to\pi^+\pi^-]}{BR[\mathrm{K_S}\to\pi^+\pi^-] + BR[\mathrm{K_L}\to\pi^+\pi^-]} \approx 0.28\%,
\end{aligned} \tag{3.5}$$

Signal-like		$\mathrm{K}\to\pi^0\pi^0$
Decay		$\mathrm{K_S K_L}\to\pi^\pm\mathrm{l}^\mp\nu\pi^0\pi^0$
1.	Tagging part selection	$N^{\mathrm{tag}}_{\mathrm{K}\to\pi^0\pi^0}$
2.	Expected number of signal-like events	$N^{\mathrm{exp}}_{\mathrm{K}\to\pi^0\pi^0} =$ $\mathrm{N}^{\mathrm{tag}}_{\mathrm{K}\to\pi^0\pi^0} \times (p_1 BR[\mathrm{K_L}\to\pi^0\pi^0] + p_2 BR[\mathrm{K_S}\to\pi^0\pi^0])$
3.	Signal-like part selection	$N^{\mathrm{sel}}_{\mathrm{K}\to\pi^0\pi^0}$
4.	Determination of efficiency	$\epsilon(\Delta t)^{\mathrm{DATA}}_{\mathrm{K}\to\pi^0\pi^0} = N^{\mathrm{sel}}_{\mathrm{K}\to\pi^0\pi^0}/N^{\mathrm{exp}}_{\mathrm{K}\to\pi^0\pi^0}$

Table 4: Algorithm to determine efficiency of $\mathrm{K}\to\pi^0\pi^0$ using $\mathrm{K_S K_L}\to\pi^\pm\mathrm{l}^\mp\nu\pi^0\pi^0$ control sample.

Branching ratios used in the algorithms to determine expected numbers of events for semileptonic case are equal to [7]:

$$\begin{aligned}
BR[K_S\to\pi^\pm l^\mp\nu] &\approx 0.12\%,\\
BR[K_L\to\pi^\pm l^\mp\nu] &\approx 67.59\%,
\end{aligned} \tag{3.6}$$

Signal-like		$\mathrm{K} \to \pi^+\pi^-$	
Decay		$\mathrm{K_S K_L} \to \pi^+\pi^- 3\pi^0$	$\mathrm{K_S K_L} \to \pi^+\pi^-\pi^+\pi^-$
1.	Tagging part selection	$N^{\mathrm{tag}}_{\mathrm{K_S}\to\pi^+\pi^-}$	$N^{\mathrm{tag}}_{\mathrm{K}\to\pi^+\pi^-}$
2.	Expected number of signal-like events	$N^{\mathrm{exp}}_{\mathrm{K}\to\pi^+\pi^-} =$ $\mathrm{N}^{\mathrm{tag}}_{\mathrm{K_S}\to\pi^+\pi^-} \times BR[\mathrm{K_S}\to\pi^+\pi^-]+$ $\mathrm{N}^{\mathrm{tag}}_{\mathrm{K}\to\pi^+\pi^-} \times (p_3 BR[\mathrm{K_L}\to\pi^+\pi^-] + p_4 BR[\mathrm{K_S}\to\pi^+\pi^-])$	
3.	Signal-like part selection	$N^{\mathrm{sel}}_{\mathrm{K_S}\to\pi^+\pi^-}$	$N^{\mathrm{sel}}_{\mathrm{K}\to\pi^+\pi^-}$
4.	Determination of efficiency	$\epsilon(\Delta t)^{\mathrm{DATA}}_{\mathrm{K}\to\pi^+\pi^-} = (N^{\mathrm{sel}}_{\mathrm{K_S}\to\pi^+\pi^-} + N^{\mathrm{sel}}_{\mathrm{K}\to\pi^+\pi^-})/N^{\mathrm{exp}}_{\mathrm{K}\to\pi^+\pi^-}$	

Table 5: Algorithm to determine efficiency of $\mathrm{K} \to \pi^+\pi^-$ using $\mathrm{K_S K_L} \to \pi^+\pi^- 3\pi^0$ and $\mathrm{K_S K_L} \to \pi^+\pi^-\pi^+\pi^-$ control samples. It is important to pay attention, that from $\mathrm{K_S K_L} \to \pi^+\pi^- 3\pi^0$ only $\mathrm{K_S} \to \pi^+\pi^-$ quantities are determined, while for $\mathrm{K_S K_L} \to \pi^+\pi^-\pi^+\pi^-$ for total $\mathrm{K} \to \pi^+\pi^-$.

while rest can be found in Table 1. It has to be said, however, that $N^{\mathrm{sel}}_{\mathrm{K}\to\pi^0\pi^0}$ is found imposing cuts under signal hypothesis, but only on neutral part. Thus, for $N^{\mathrm{sel}}_{\mathrm{K}\to\pi^+\pi^-}$ and $N^{\mathrm{sel}}_{\mathrm{K_S}\to\pi^+\pi^-}$ only cuts tied with charged part are used. They do not include, however, the ones connected with the kinematic fit under signal hypothesis, as it correlates both parts of the event. It is assumed, that all selection conditions are independent of each other, so the calculation of $f(\Delta t)$ can be done at the earlier stage. Under this assumption $f(\Delta t)$ could be applied to the actual MC efficiency with all the cuts involved.

Efficiencies for $\mathrm{K} \to \pi^+\pi^-$ and $\mathrm{K} \to \pi^0\pi^0$ are in principle mutually independent, as they are calculated from independent control samples. This allows to calculate a total efficiency as:

$$\epsilon(\Delta t)^{\mathrm{DATA}}_{\mathrm{K_S K_L}\to\pi^+\pi^-\pi^0\pi^0} = \epsilon(\Delta t)^{\mathrm{DATA}}_{\mathrm{K}\to\pi^+\pi^-} \times \epsilon(\Delta t)^{\mathrm{DATA}}_{\mathrm{K}\to\pi^0\pi^0}, \tag{3.7}$$

and simultaneously for Monte Carlo with the use of the control samples as:

$$\epsilon(\Delta t)^{\mathrm{MC}}_{\mathrm{K_S K_L}\to\pi^+\pi^-\pi^0\pi^0} = \epsilon(\Delta t)^{\mathrm{MC}}_{\mathrm{K}\to\pi^+\pi^-} \times \epsilon(\Delta t)^{\mathrm{MC}}_{\mathrm{K}\to\pi^0\pi^0}, \tag{3.8}$$

Having it determined, the final step is to calculate a proper correction factor using the formula:

$$f(\Delta t) = \epsilon(\Delta t)^{\mathrm{DATA}}_{\mathrm{K_S K_L}\to\pi^+\pi^-\pi^0\pi^0} / \epsilon(\Delta t)^{\mathrm{MC}}_{\mathrm{K_S K_L}\to\pi^+\pi^-\pi^0\pi^0}, \tag{3.9}$$

which is the result of this thesis.

4 Determination of control samples and results

In the following section, firstly I focus on the specification of data sets used in the analysis, along with applied filtering algorithms. Moreover, the choice of selection conditions for control samples is justified and finally cuts under the signal hypothesis are imposed. Finally the correction factor $f(\Delta t)$ is determined.

4.1 Chosen decay channels for control samples

As was mentioned earlier, the total integrated luminosity of KLOE experiment was $2.5\ \mathrm{fb}^{-1} = 0.8\ \mathrm{fb}^{-1} + 1.7\ \mathrm{fb}^{-1}$ for runs 2001-2002 and 2004-2005, respectively. In this thesis 2001-2002 run is not used due to its worse resolution quality, so all results are based on 2004-2005 part. There are used Monte Carlo and collected DATA events corresponding to run range 30300-41902. A plot revealing integrated luminosity collected for KLOE experiment in successive years is shown in Fig. 11.

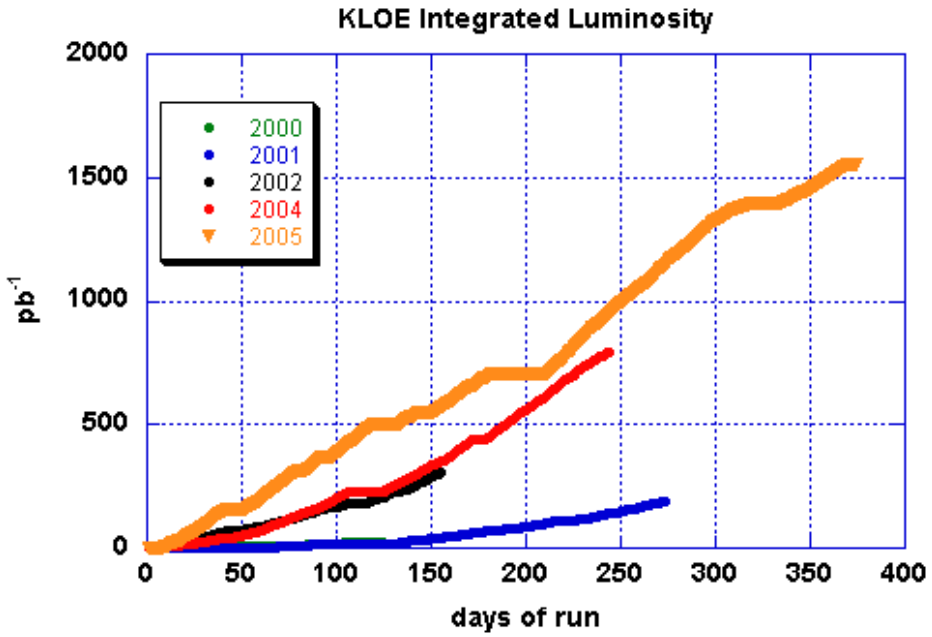

Fig. 11: Integrated luminosity for successive years of DAΦNE operation for KLOE experiment. Figure adapted from [26].

The actual set of events used in the analysis corresponding to $1\times$ luminosity for DATA ($1\times 1.7\ \mathrm{fb}^{-1}\times 30\% = 0.51\ \mathrm{fb}^{-1}$) and $2\times$ luminosity for Monte Carlo ($2\times 1.7\ \mathrm{fb}^{-1}\times 70\% = 2.38\ \mathrm{fb}^{-1}$) due to a generation providing greater statistics. The 30% and 70% factors are due to the technical problem of accessing the tape library with DATA and MC samples at the time of preparation of this thesis.

To save disk space and provide preselected channels for specific analyses lead in KLOE experiment, an initial filtering is applied. Events are assigned by ECL algorithm (Event CLassification algorithm) to *streams* divided further into tagging sub-algorithms. Technically, they are sets of physical conditions, which maximize the probability, that a given event has properties assumed in a tag. I take under consideration the KSL stream, which is divided into:

- KSTAG $\Rightarrow$ $\mathrm{K_L}$ decay was detected,
- KLTAG $\Rightarrow$ $\mathrm{K_S} \to \pi^+\pi^-$ decay was detected,
- KSNEUT $\Rightarrow$ $\mathrm{K_S} \to \pi^0\pi^0$ decay was detected,
- KLCRASH $\Rightarrow$ $\mathrm{K_L}$ in EMC interaction was found,
- KSEMIL $\Rightarrow$ event is a candidate for $\mathrm{K_S} \to \pi \mathrm{l} \nu$ decay,
- KLNEUT $\Rightarrow$ $\mathrm{K_L} \to 3\pi^0$ decay was detected,
- INTERTAG $\Rightarrow$ event is a good candidate for interferometric studies,
- KLPPPTAG $\Rightarrow$ $\mathrm{K_L} \to \pi^+\pi^-\pi^0$ was found independently of $\mathrm{K_S}$.

If any of these tags is fulfilled for a given event, it is assigned to the KSL stream. The detailed description of tagging algorithms, along with all physical constraints, can be found in [34]. It is worth mentioning, that streams are not exclusive within their conditions, so a given event can be assigned to a few streams.

4.2 Conditions of the selection

Before approaching the actual analysis, it is worth to define some quantities, which will be used frequently. The first one is the 4-momentum of a particle used in a convention:

$$\begin{aligned} \mathbf{p}_n &= (E(m_n), \vec{p}_n), \\ E(m_n) &= \sqrt{m_n^2 + \vec{p}_n^2}, \\ \vec{p}_n &= (p_n^x, p_n^y, p_n^z), \end{aligned} \tag{4.1}$$

where $\vec{p}_n$ stands for spatial momentum of n-th particle and $E(m_n)$ - for the energy of an n-th particle with mass m. Masses of particles used during the studies are listed in a Table 6 [7].

Mass	Value [$\mathrm{MeV/c^2}$]	Error [$\mathrm{MeV/c^2}$]
m_{ϕ}	1019.461	0.016
$m_{\mathrm{K_0}}$	497.611	0.013
m_{π^0}	134.9768	0.0005
$m_{\pi^{\pm}}$	139.57039	0.00018

Table 6: Masses of particles used during the studies. Values and uncertainties can be found in [7].

Second aspect are the variables of registered EMC clusters. They can be uniquely characterized via space-time 4-vectors:

$$\mathbf{V}_{\mathrm{cl},i} = \begin{pmatrix} T_{\mathrm{cl},i} \\ X_{\mathrm{cl},i} \\ Y_{\mathrm{cl},i} \\ Z_{\mathrm{cl},i} \end{pmatrix}, \tag{4.2}$$

where $T_{\mathrm{cl},i}$ is a *cluster time* of i-th cluster, i.e. time passed since collision at IP until activation of the i-th cluster, while $\vec{V}_{\mathrm{cl},i} = (X_{\mathrm{cl},i}, Y_{\mathrm{cl},i}, Z_{\mathrm{cl},i})$ stands for the spatial position of a *cluster's centroid* with respect to the geometrical center of DC. Moreover, an energy of a cluster is indicated as $E_{\mathrm{cl},i}$.

4.2.1 Reconstruction and selection of $\mathrm{K_S K_L} \to \pi^+\pi^-\pi^0\pi^0$ events

The basis of the studies is $\mathrm{K_S K_L} \to \pi^+\pi^-\pi^0\pi^0$ channel, which is reconstructed using two main algorithms. First one is focused on the best choice of $\mathrm{K} \to \pi^+\pi^-$ vertex, conditions are shown below:

- at least 1 charged vertex in an analyzed event,
- exactly 2 tracks with opposite signs connected to the vertex,
- vertex, for which invariant mass of tracks is closest to $m_{\mathrm{K_0}}$, is chosen as the origin of $\pi^+\pi^-$.

This method results in the reconstructed kaon's 4-momentum $\mathbf{p}^{\mathrm{rec}}_{\mathrm{K}\to\pi^+\pi^-}$ as a sum of two reconstructed momenta under assumption of $m_{\pi^{\pm}}$. The invariant mass spectrum is visible for all considered channels in Fig. 12.

To improve the resolution of an energy, the hypothesis of 2 body decay, due to $\phi \to \mathrm{K_S K_L}$, can be used. This so-called *boost method* is derived in Appendix B and finally gives $\mathbf{p}^{\mathrm{boost}}_{\mathrm{K}\to\pi^+\pi^-}$, which is a starting point for the reconstruction of a neutral

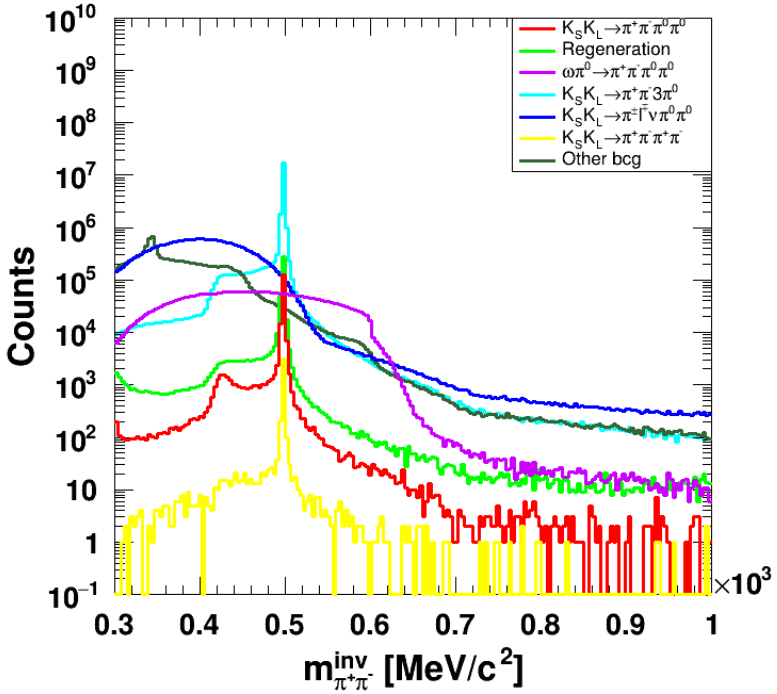

Fig. 12: Reconstructed invariant mass of $\mathrm{K} \to \pi^+\pi^-$ using an algorithm described above. Decays fulfilling the condition of 2 body decay are centered around m_{K_0}.

$\mathrm{K} \to \pi^0\pi^0$ vertex. It is possible to determine a 4-momentum of $\mathrm{K} \to \pi^0\pi^0$ as:

$$\mathbf{p}_{K\to\pi^0\pi^0} = \mathbf{p}_\phi - \mathbf{p}^{\mathrm{boost}}_{K\to\pi^+\pi^-}, \tag{4.3}$$

using total 4-momentum conservation and worth mentioning is, that $\mathbf{p}_\phi$ is an average 4-momentum determined run by run using Bhabha scattering events measured during the calibration. Reconstruction of a neutral vertex is done using *the time of flight algorithm* (details can be found in Appendix C) and the invariant mass of 4γ is visible in Fig. 13.

It can be seen, that for $\mathrm{K_S K_L} \to \pi^+\pi^-\pi^0\pi^0$ peak is centered around m_{K_0}, but with worse resolution, than for invariant mass of charged pions. For $\mathrm{K_S K_L} \to \pi^\pm \mathrm{l}^\mp \nu\pi^0\pi^0$ it is worth noticing, that even when it has a decay $\mathrm{K} \to \pi^0\pi^0$, a bad reconstruction of momentum using an algorithm mentioned earlier has an impact on the determination of proper clusters and its peak is shifted. Finally, kaons' proper times at the moment of decay are determined for both vertices and Δt can be calculated all these variables are shown in Fig. 14.

It can be seen, that the proper times are peaked around zero, but extend farther, because $\mathrm{K_S}$ and $\mathrm{K_L}$ are mixed in both charged and neutral decays. Interference pattern in $\mathrm{K_S K_L} \to \pi^+\pi^-\pi^0\pi^0$ Δt distribution is introduced directly via Eq. (5.10). Values of this function act as weights for a given Δt during filling of the histogram. Finally, it has to be renormalized to the number of events of an initial, unweighted $\mathrm{K_S K_L} \to \pi^+\pi^-\pi^0\pi^0$

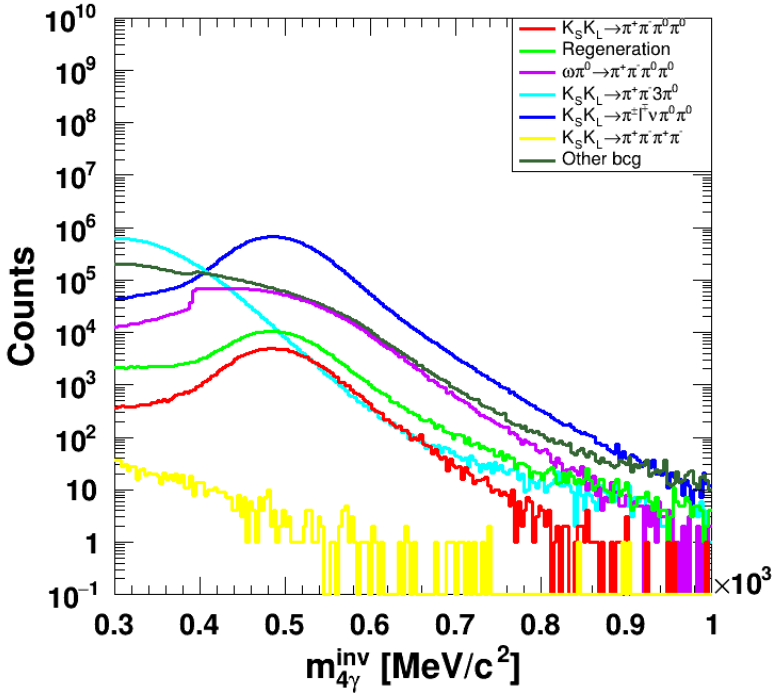

Fig. 13: Reconstructed invariant mass of $\mathrm{K} \to 4\gamma$ using time of flight algorithm. Decays fulfilling the condition of 4γ hypothesis are centered around m_{K_0}, but with worse resolution than in the $m^{inv}_{\pi^+\pi^-}$ case.

histogram details can be found in [1]. It is not clearly visible in Fig. 14, because of a used logarithmic scale.

For the completeness, it is worth mentioning, that after the reconstruction the kinematic fit under the signal hypothesis is applied. It uses a least-squares method, described for example in [35, 36], with 36 free parameters, among which are:

- curvature, azimuthal angle and cotangent of the polar angle of two charged tracks (2×3),
- $E_{cl,i}$, $X_{cl,i}$, $Y_{cl,i}$, $Z_{cl,i}$, $T_{cl,i}$ for each photon (4×5),
- Neutral vertex and IP coordinates (2×3),
- 4-momentum of ϕ meson (1×4).

Physical constraints are imposed via Lagrange multipliers for 10 conditions:

- time of flight of photons from neutral vertex to cluster's centroid (4),
- 4-momentum conservation of a system (4),
- invariant mass of $\pi^+\pi^-$ equal to m_{K_0} (1),

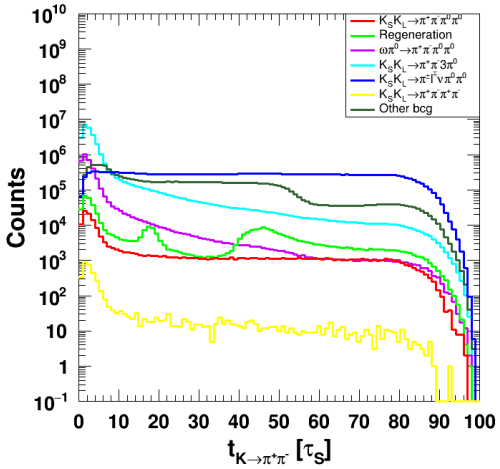

(a) Proper time of kaon from $\mathrm{K} \to \pi^+\pi^-$. Due to much bigger abundance of $\mathrm{K_L} \to \pi^\pm \mathrm{l}^\mp \nu$ peak around zero is not visible for $\mathrm{K_S K_L} \to \pi^\pm \mathrm{l}^\mp \nu \pi^0 \pi^0$.

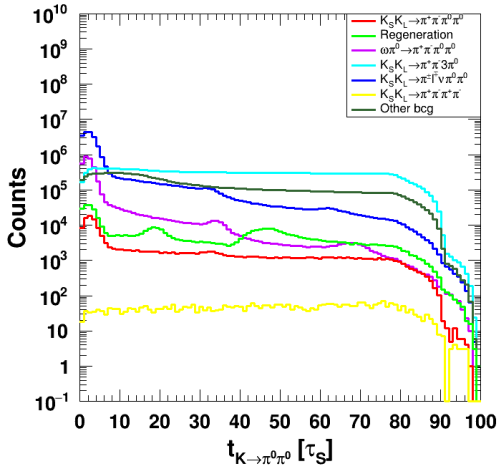

(b) Proper time of kaon from $\mathrm{K} \to \pi^0\pi^0$. $\mathrm{K_S K_L} \to \pi^+\pi^- 3\pi^0$ contains only $\mathrm{K_L} \to \pi^0\pi^0$, so the peak around zero is not visible.

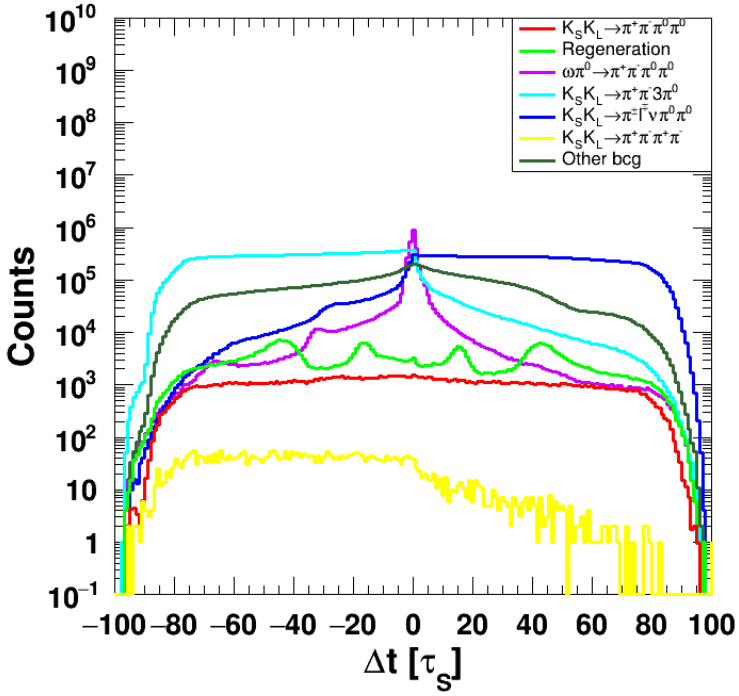

(c) Δt calculated from reconstructed kaons' proper times. Minimum in the center of $\mathrm{K_S K_L} \to \pi^+\pi^-\pi^0\pi^0$ is not visible due to limited resolution of reconstruction.

Fig. 14: Reconstructed kaons' proper times at the time of decay and Δt for all channels taken for the analysis. Via (a) and (b) it can be seen, that both decays consist of a mixture of $\mathrm{K_S}$ and $\mathrm{K_L}$, which is predicted by corresponding branching ratios from Table 1.

- invariant mass of 4γ equal to $m_{\mathrm{K_0}}$ (1).

This kinematic fit is used both for the adjustment of the parameters and rejection of events, which fulfill $\mathrm{K_S K_L} \to \pi^+\pi^-\pi^0\pi^0$ hypothesis the worst. In this thesis, however, only reconstructed variables (kin. fit not in use) will be used to determine efficiencies, due to the character of control samples, which require independence.

Finally, studies in [1] revealed the optimal cuts to use for $\mathrm{K_S K_L} \to \pi^+\pi^-\pi^0\pi^0$ selection they are gathered in Table 7. For the purposes of this thesis, they could be divided into two classes acting on $\mathrm{K} \to \pi^+\pi^-$ or acting on $\mathrm{K} \to \pi^0\pi^0$. Conditions using fitted variables are not involved here.

$\mathrm{K} \to \pi^+\pi^-$	$\mathrm{K} \to \pi^0\pi^0$
$\lvert m^{inv}_{\pi^+,\pi^-} - m_{\mathrm{K_0}}\rvert < 1.2\ \mathrm{MeV/c^2}$	$\lvert m^{inv}_{4\gamma} - m_{\mathrm{K_0}}\rvert < 76\ \mathrm{MeV/c^2}$
$Q_{miss} < 3.75\ \mathrm{MeV}$	$t_{r,sum} > -1$
$\cos\alpha_{\pi^+\pi^-} < -0.8$ (in CM frame of kaon)	-

Table 7: Optimal cuts chosen under $\mathrm{K_S K_L} \to \pi^+\pi^-\pi^0\pi^0$ hypothesis (without fitted variables) can be found in [1].

α_{π^+,π^-} stands for the angle between reconstructed charged pions' tracks and $t_{r,sum}$ is equal to:

$$t_{r,sum} = \sum_{i=1}^{4}\left[T_{cl,i} - \frac{||\vec{V}_{cl,i} - \vec{V}_{\mathrm{neu}}||}{c} - \frac{||\vec{V}_{\mathrm{neu}} - \vec{V}_{\mathrm{IP}}||}{v_{\mathrm{K}}}\right], \tag{4.4}$$

where v_{K} is a velocity of kaon decaying into $\mathrm{K} \to \pi^0\pi^0$. Moreover, considering $\mathrm{K} \to \pi^+\pi^-$, Q_{miss} stands for the missing 4-momentum comparing reconstructed and corrected via boost method 4-momenta of kaon, which can be expressed as:

$$Q_{miss} = ||\mathbf{p}^{\mathrm{rec}}_{\mathrm{K}\to\pi^+\pi^-} - \mathbf{p}^{\mathrm{boost}}_{K\to\pi^+\pi^-}||, \tag{4.5}$$

and as it is calculated in Minkowski's metric, it is a Lorentz invariant quantity.

After getting the proper overview of the signal selection, the corresponding control samples can be considered.

4.2.2 Selection of $\mathrm{K_S K_L} \to \pi^\pm l^\mp \nu \pi^0\pi^0$ events

The first control sample taken into account is the one tied with $\mathrm{K_S K_L} \to \pi^\pm l^\mp \nu \pi^0\pi^0$ events. Tagging decay in this context is $\mathrm{K} \to \pi^\pm l^\mp \nu$ and the signal-like is $\mathrm{K} \to \pi^0\pi^0$, so this channel saturates all possible situations for the neutral part.

As was mentioned in the previous section, selection is divided into two stages: selection of a pure $\mathrm{K_S K_L} \to \pi^\pm l^\mp \nu \pi^0\pi^0$ sample using tagging decay's properties and then imposing the conditions under the $\mathrm{K} \to \pi^0\pi^0$ hypothesis. It can be noticed, that the tagging part is in fact a 3 body event, where the neutrino, due to its interaction cross-section, is not

registered and flies away with a fraction of $\sqrt{s}$. It is especially visible in Q_{miss}. Charged vertex here is chosen according to the method described in the last subsection. The inherent sense of this variable in the context of semileptonic sample is tied with the assumption of 2 body decay, both in reconstruction of charged vertex and the boost method. The actual cut was chosen by the use of a sampled plot of efficiency and purity for $\mathrm{K_S K_L} \to \pi^{\pm} \mathrm{l}^{\mp} \nu \pi^0 \pi^0$ decay actual spectra and plots can be seen in Fig. 15. The cut range is determined to:

$$|Q_{miss} - 71.13\ \mathrm{MeV}| < 25\ \mathrm{MeV}. \tag{4.6}$$

so that every event beyond it is rejected. Purity along with the efficiency after this cut are equal to:

$$\mathrm{Purity} = 74.65\%,\ \epsilon_{\mathrm{K_S K_L} \to \pi^{\pm} \mathrm{l}^{\mp} \nu \pi^0 \pi^0} = 27.14\%. \tag{4.7}$$

Another variable, which keeps information about 3 body decay in $\mathrm{K_S K_L} \to \pi^{\pm} \mathrm{l}^{\mp} \nu \pi^0 \pi^0$ is α_{π^+,π^-}, i.e., angle between π^+ and π^- in the CM frame of kaon. For 2 body decay it should be peaked at $180°$, as π^+ and π^- are kinematically identical, while for 3 body decay it is shifted. The choice of cut is justified by efficiency and purity plots both distributions and graphs for all channels are visible in Fig. 16. In this context, the cut range was chosen as:

$$|\alpha_{\pi^+,\pi^-} - 145.8°| < 10°. \tag{4.8}$$

so that every event beyond it is rejected. Purity along with the efficiency after this cut are equal in the end to:

$$\mathrm{Purity} = 81.06\%,\ \epsilon_{\mathrm{K_S K_L} \to \pi^{\pm} \mathrm{l}^{\mp} \nu \pi^0 \pi^0} = 12.08\%. \tag{4.9}$$

This cut actually ends the stage of tagging part selection for $\mathrm{K_S K_L} \to \pi^{\pm} \mathrm{l}^{\mp} \nu \pi^0 \pi^0$ and the $\mathrm{K_S K_L} \to \pi^+ \pi^- \pi^0 \pi^0$ hypothesis conditions can be imposed.

$\mathrm{K} \to \pi^0 \pi^0$ cannot be reconstructed here using time of flight method, because of the independence condition between tagging and signal-like part for control samples. This is resolved by a *trilateration method*, which was developed in the context of KLOE in [37] and its description for the purpose of these studies is available in Appendix D. It uses only information about clusters themselves without momentum direction of $\mathrm{K} \to \pi^+ \pi^-$, so the condition is fulfilled. A set of 4 clusters, which best suits $\mathrm{K} \to \pi^0 \pi^0 \to 4\gamma$ the hypothesis, corresponds to the minimal $|m^{inv}_{4\gamma} - m_{\mathrm{K_0}}|$ for a given event. Only events, for which a formal solution exists (conditions listed in Appendix D) are taken for a further analysis. Thus, efficiency and purity of $\mathrm{K_S K_L} \to \pi^{\pm} \mathrm{l}^{\mp} \nu \pi^0 \pi^0$ after this step are:

$$\mathrm{Purity} = 74.67\%,\ \epsilon_{\mathrm{K_S K_L} \to \pi^{\pm} \mathrm{l}^{\mp} \nu \pi^0 \pi^0} = 3.11\%. \tag{4.10}$$

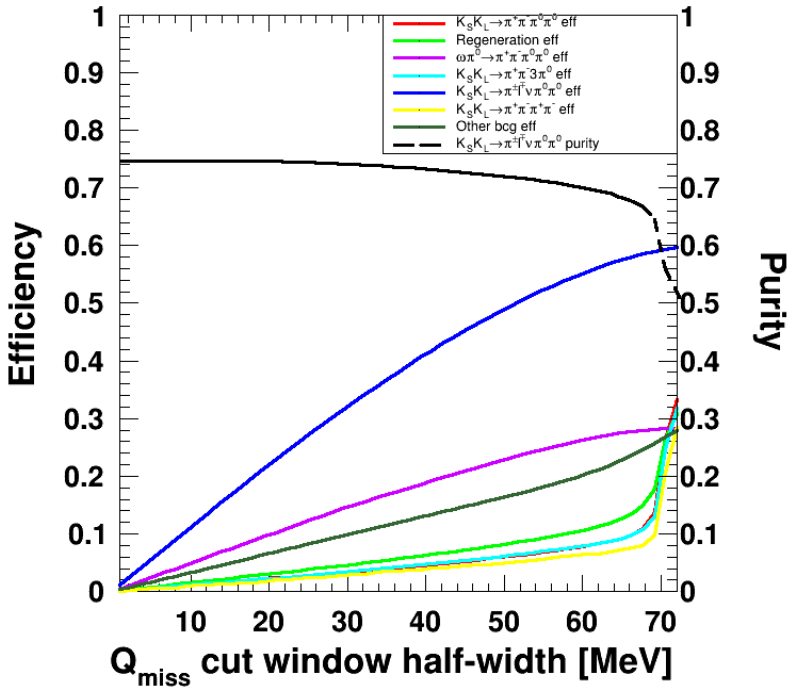

(a) Efficiency and purity plots used to determine symmetric cut. The half-width of a cut window was chosen to 25 MeV due to the stability of a predicted purity.

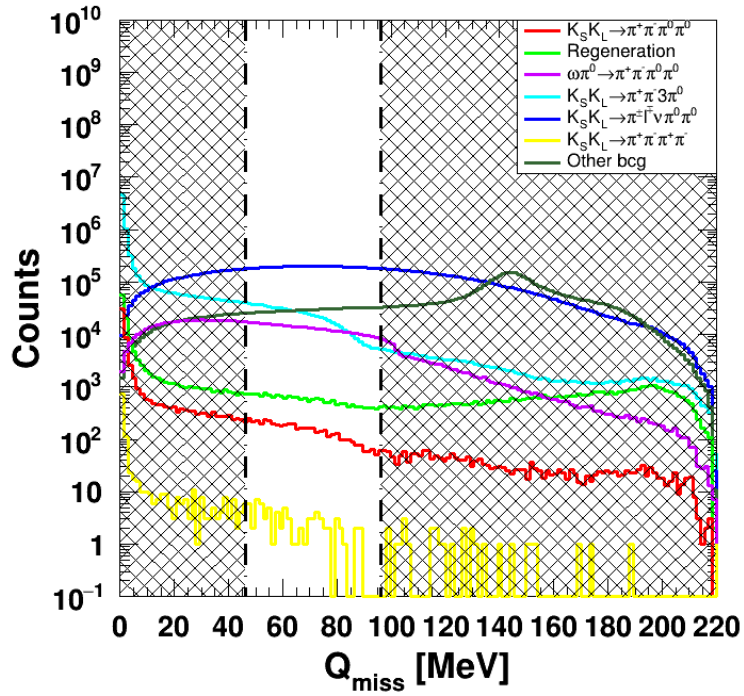

(b) Distributions of a Q_{miss} variables for all channels. Vertical lines stand for the symmetric cut events beyond them are rejected.

Fig. 15: Plots for Q_{miss} variable used in the analysis.

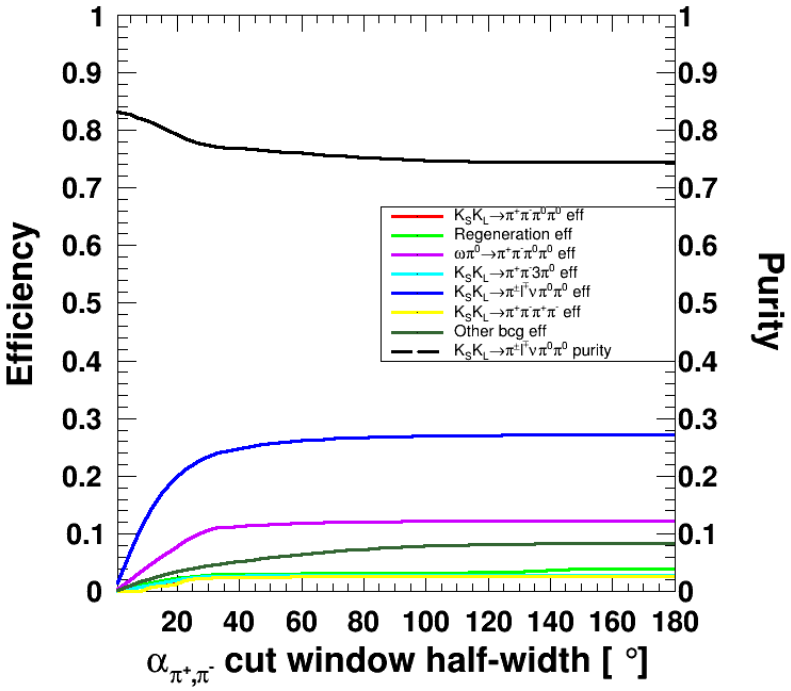

(a) Efficiency and purity plots used to determine symmetric cut. Cut windows' half-width 10° was chosen due to the value and stability of a predicted purity.

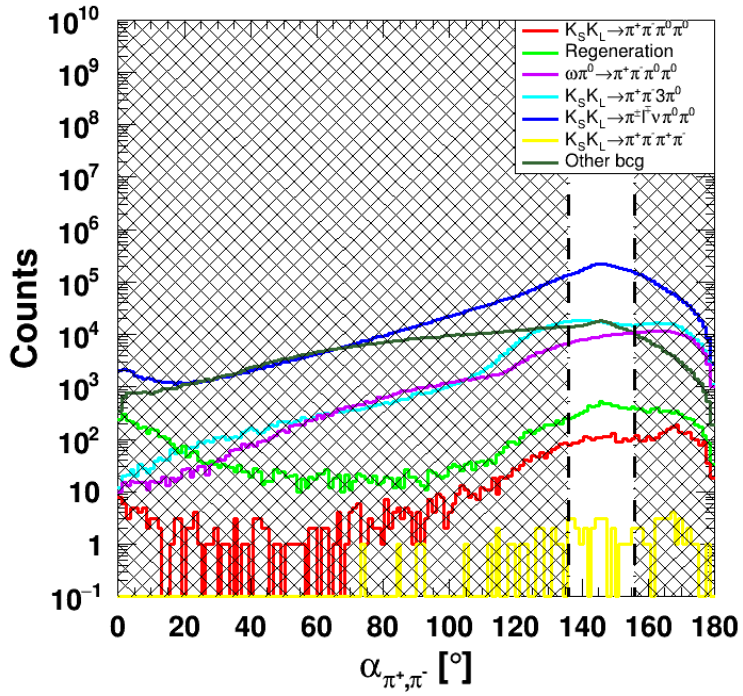

(b) Distributions of a α_{π^+,π^-} variable for all channels. Vertical lines stand for the symmetric cut events beyond them are rejected.

Fig. 16: Plots for α_{π^+,π^-} variable used in the analysis.

Using neutral vertex determined with trilateration algorithm and charged vertex reconstructed with an algorithm described in the previous subsection, paths of kaons can be found along with Δt. They are visible in Fig. 17. Here can be seen a different shape of distributions w.r.t. Fig. 14, e.g., broadened ω peak. It can be caused both by the imposed cuts during tagging selection, but also by worse resolution of trilateration for 4γ, than in the time of flight method. This should be kept in mind for the purpose of efficiency analyses.

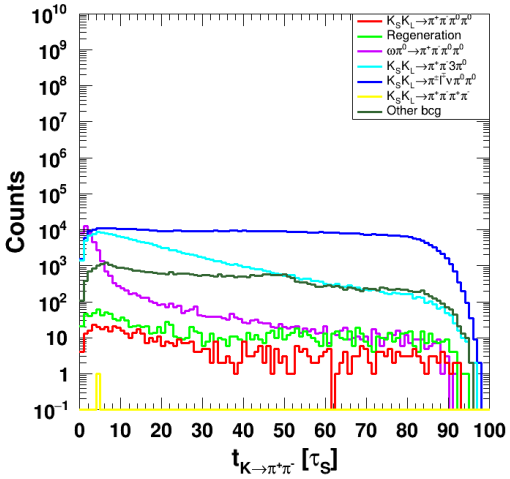

(a) Path of kaon from $\mathrm{K} \to \pi^+\pi^-$.

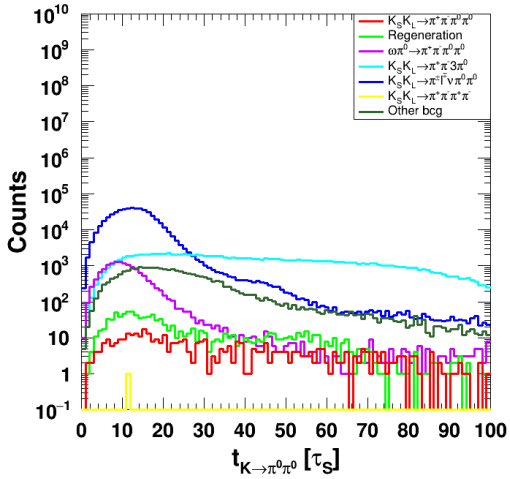

(b) Path of kaon from $\mathrm{K} \to \pi^0\pi^0$.

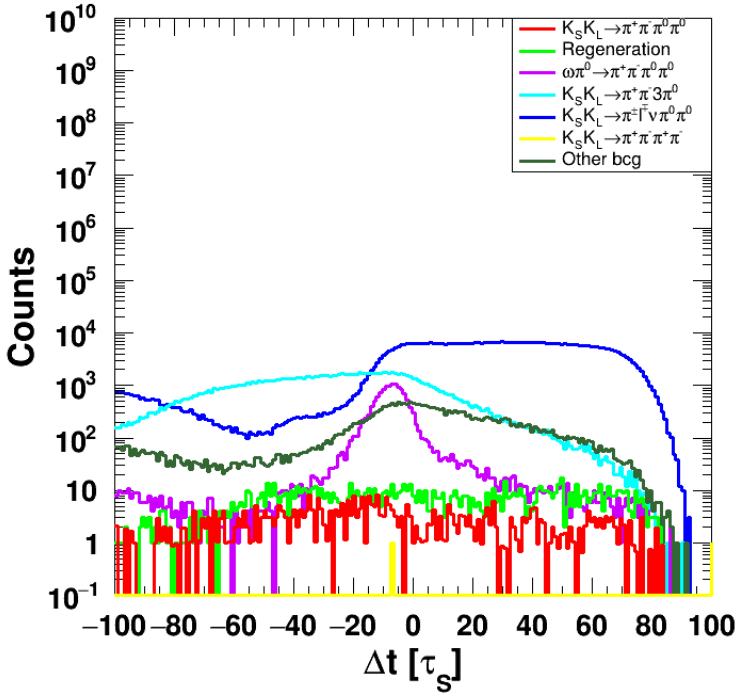

(c) Δt calculated from reconstructed kaons' paths using trilateration method.

Fig. 17: Reconstructed kaons' paths and Δt for all channels taken for the analysis. Via (a) and (b) it can be seen, that both decays consist of a mixture of $\mathrm{K_S}$ and $\mathrm{K_L}$, which is predicted by corresponding branching ratios from Table 1.

This point ends the selection of $\mathrm{K_S K_L} \to \pi^{\pm} \mathrm{l}^{\mp} \nu \pi^0 \pi^0$. The actual considerations about efficiencies basing on Table 4 will be continued in the next subsection.

4.2.3 Selection of $\mathrm{K_S K_L} \to \pi^+ \pi^- 3\pi^0$ events

For this control sample, the tagging part is $\mathrm{K_L} \to 3\pi^0$, while the signal-like is $\mathrm{K_S} \to \pi^+ \pi^-$. Due to the independence, the trilateration method has to be used one more time, but for 6γ case it is described in Appendix D. It does not use information about the invariant mass of kaon, but only the geometrical constraints for all 6 clusters, so it does not impose the additional hypothesis to the selection of $\mathrm{K_L} \to 3\pi^0$. To reject events, which poorly suit this hypothesis, an additional cut is imposed on a total spread, R, of 15 trilateration solutions of all possible combinations of 4 out of 6 clusters. basing on efficiency and purity plot results are visible in Fig. 18.

After the application of trilateration method, the purity and efficiency for $\mathrm{K_S K_L} \to \pi^+ \pi^- 3\pi^0$ sample are equal to:

$$\mathrm{Purity} = 98.10\%, \ \epsilon_{\mathrm{K_S K_L} \to \pi^+ \pi^- 3\pi^0} = 26.29\%. \tag{4.11}$$

Similarly to the previous case, a neutral vertex has to be found using a trilateration algorithm for the potential 4γ set. This will provide the independence of reconstruction between neutral and charged vertices. In this case, kaons' paths and the resulting time difference are shown in Fig. 19. Similarly, as for $\mathrm{K_S K_L} \to \pi^{\pm} \mathrm{l}^{\mp} \nu \pi^0 \pi^0$ different shape of distributions is visible. Thus, earlier conclusions are also appropriate here.

Just like before, this point ends the selection of $\mathrm{K_S K_L} \to \pi^+ \pi^- 3\pi^0$ channel. Further analysis concerning determination of efficiencies will be continued in the next subsection.

4.2.4 Selection of $\mathrm{K_S K_L} \to \pi^+ \pi^- \pi^+ \pi^-$ events

Finally, to complete the control sample for $\mathrm{K} \to \pi^+ \pi^-$, the selection of $\mathrm{K_S K_L} \to \pi^+ \pi^- \pi^+ \pi^-$ can be performed. It is a CP violating channel, so number of events is very low, however, due to existence of $\mathrm{K_L} \to \pi^+ \pi^-$ it is a supplement to an already selected $\mathrm{K_S K_L} \to \pi^+ \pi^- 3\pi^0$ control sample. The algorithm of selection here is based on a few main points:

1. Only events with at least two vertices, each with exactly two tracks, are taken into consideration.

2. Fiducial volume around an averaged run by run IP selection: $R_T < 10$ cm and $|z_{\mathrm{ch}} - z_{\mathrm{IP}}| < 20$ cm

3. Iteration over all vertices. Vertex is chosen if it lies *inside* the fiducial volume and its $m^{inv}_{\pi^+\pi^-,1}$ is closest to $m_{\mathrm{K_0}} \Rightarrow \mathrm{K_1}$ kaon reconstruction (good candidate for $\mathrm{K_S}$).

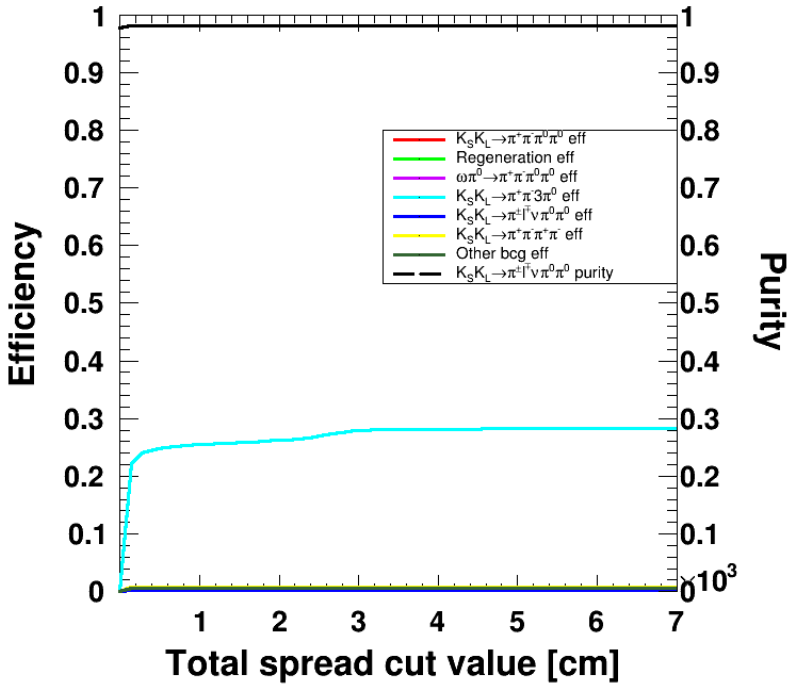

(a) Efficiency and purity plots for cut on total spread of solutions.

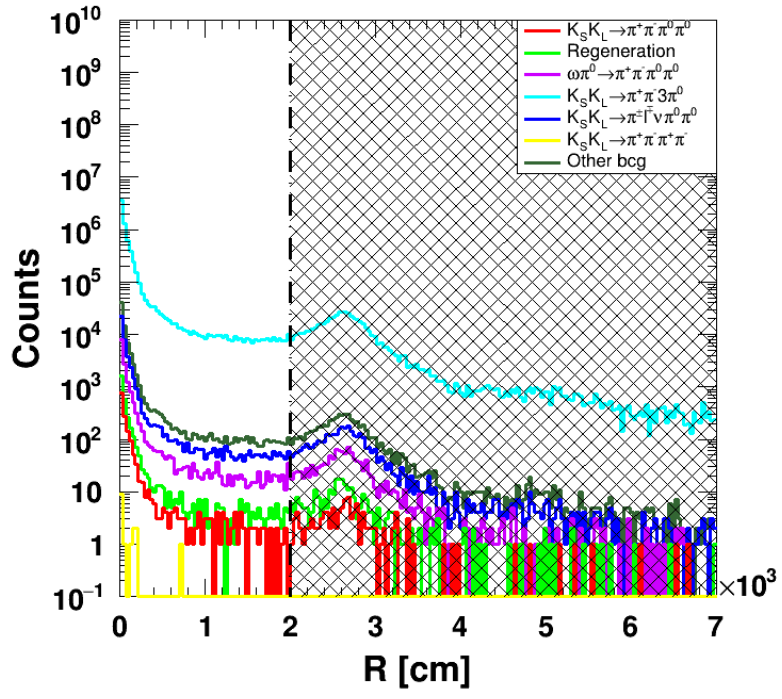

(b) Total spread with an indicated rejected region.

Fig. 18: Efficiency-purity plot and a total spread histogram with an indicated rejected region. The sharp peak around zero stands for the very well reconstructed events.

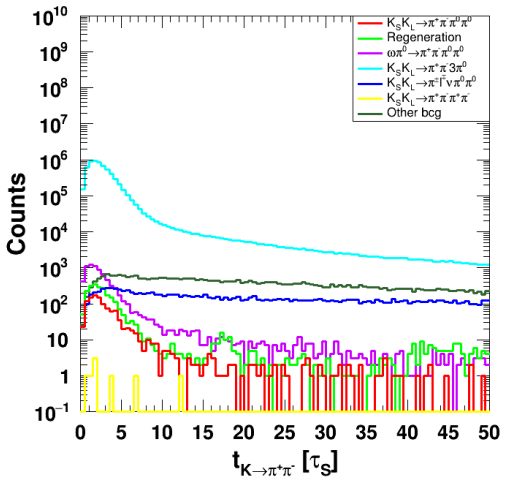

(a) Proper time of kaon from $\mathrm{K_S} \to \pi^+\pi^-$. For $\mathrm{K_SK_L} \to \pi^+\pi^-3\pi^0$ it corresponds to $\mathrm{K_S} \to \pi^+\pi^-$

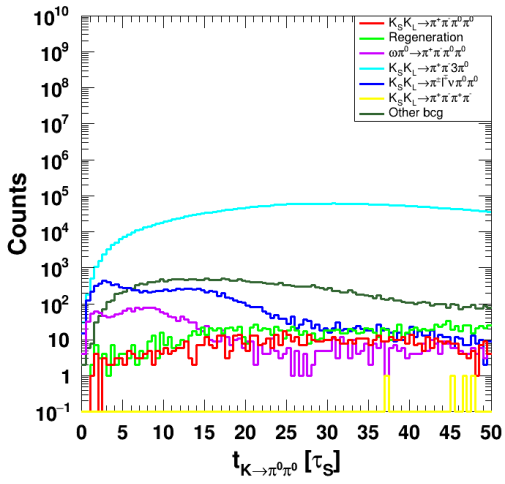

(b) Proper time of kaon from neutral decay. It is worth noticing, that it corresponds only to $\mathrm{K_L} \to \pi^0\pi^0$ for $\mathrm{K_SK_L} \to \pi^+\pi^-3\pi^0$ histogram.

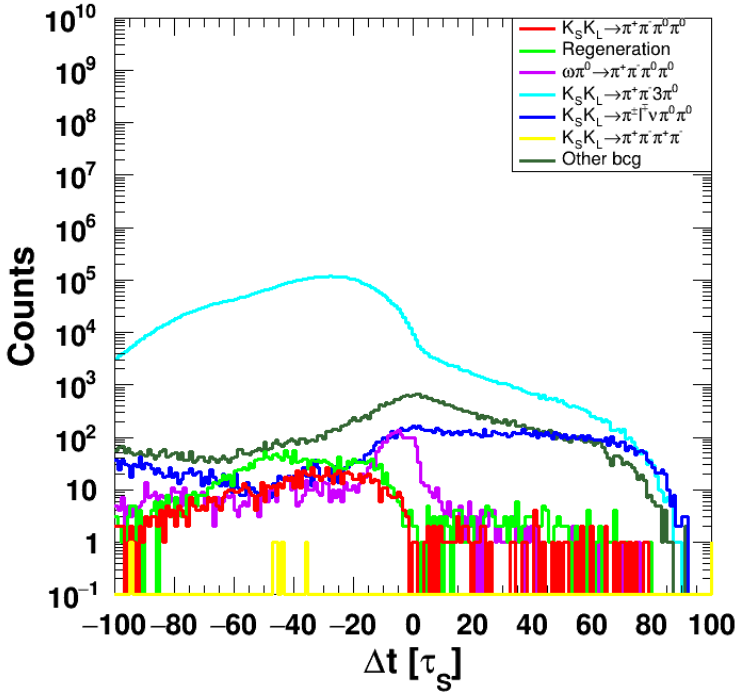

(c) Δt calculated from reconstructed kaons' proper times using trilateration method.

Fig. 19: Reconstructed kaons' proper times and Δt for all channels taken for the analysis. Via (a) and (b) it can be seen, that both decays consist of a mixture of $\mathrm{K_S}$ and $\mathrm{K_L}$, which is predicted by corresponding branching ratios from Table 1.

4. Iteration over vertices in the entire detector, besides the one chosen for $\mathrm{K_1}$. Vertex with $m^{inv}_{\pi^+\pi^-,2}$ closest to $m_{\mathrm{K_0}}$ is taken $\Rightarrow$ $\mathrm{K_2}$ kaon reconstruction (good candidate for $\mathrm{K_L}$).

5. Event taken for the further analysis if both K_1 and K_2 were reconstructed properly.

R_T here stands for the transversal radius, but calculated w.r.t an averaged run by run IP, i.e. $R_T = \sqrt{(x_{\mathrm{ch}} - x_{\mathrm{IP}})^2 + (y_{\mathrm{ch}} - y_{\mathrm{IP}})^2}$ and ch subscript indicates the charged vertex. Conditions for the fiducial volume are based on the maximum length, which can be covered by, K_S according to MC generated events.

Invariant masses of both reconstructed kaons are visible in Fig. 20. As selection can

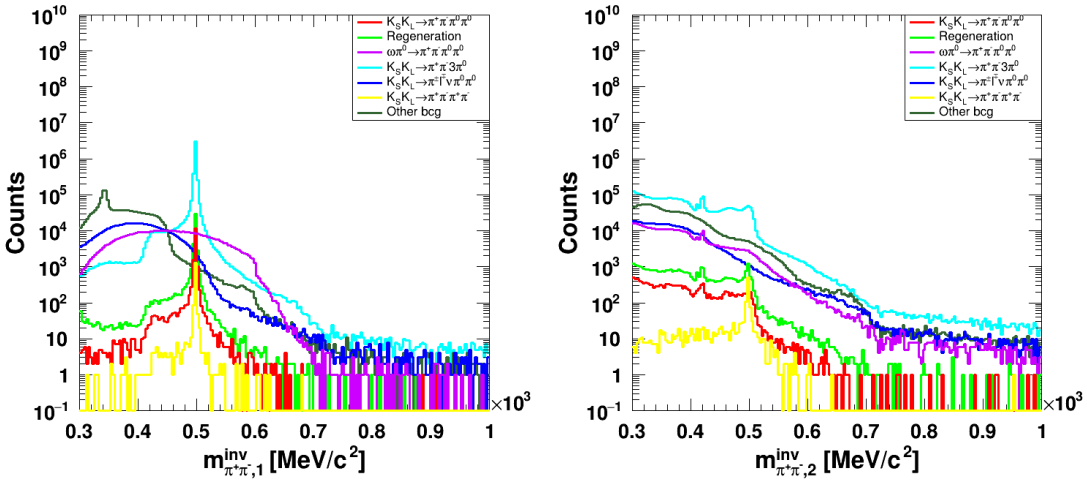

(a) Invariant mass of K_1.

(b) Invariant mass of K_2.

Fig. 20: Invariant masses of kaons reconstructed using the described algorithm. It can be seen, that for $\mathrm{K_S K_L} \to \pi^+\pi^-\pi^+\pi^-$, both are sharply peaked around m_{K_0}.

be performed only on $\mathrm{K}_1 \to \pi^+\pi^-$, it was chosen to cut $m^{inv}_{\pi^+\pi^-,1}$ symmetrically around m_{K_0}. Rejection should be possible at an efficiency of $\sim$30%, but due to the low abundance of $\mathrm{K_S K_L} \to \pi^+\pi^-\pi^+\pi^-$ channel w.r.t other ones the purity is low. Cut value was set to:

$$|m^{inv}_{\pi^+\pi^-,1} - m_{\mathrm{K}_0}| < 2\ \mathrm{MeV/c^2}, \tag{4.12}$$

to reject as many background events as possible without lowering the efficiency of $\mathrm{K_S K_L} \to \pi^+\pi^-\pi^+\pi^-$. Efficiency-purity plots and histogram of $m^{inv}_{\pi^+\pi^-}$ with indicated rejected regions can be found in Fig. 21. Finally, efficiency and purity for $\mathrm{K_S K_L} \to \pi^+\pi^-\pi^+\pi^-$ are equal to:

$$\mathrm{Purity} = 0.04\%,\ \epsilon_{\mathrm{K_S K_L} \to \pi^+\pi^-\pi^+\pi^-} = 32.05\%. \tag{4.13}$$

This channel needs a redefinition of Δt, because trilateration would, in fact, give a combination of clusters, which for sure are not originating in a neutral decay of kaon. For this purpose, it is assumed, that due to the very good resolution of charged vertices' coordinates, they can be always assigned to $\mathrm{K_S}$ or $\mathrm{K_L}$, depending on which vertex was registered

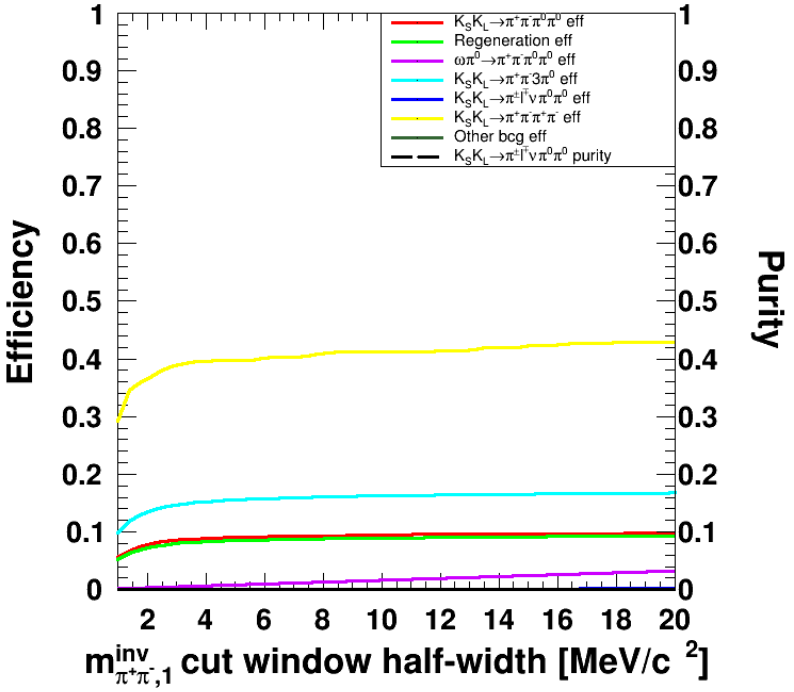

(a) Efficiency and purity plots for cut on $m^{inv}_{\pi^+\pi^-,1}$.

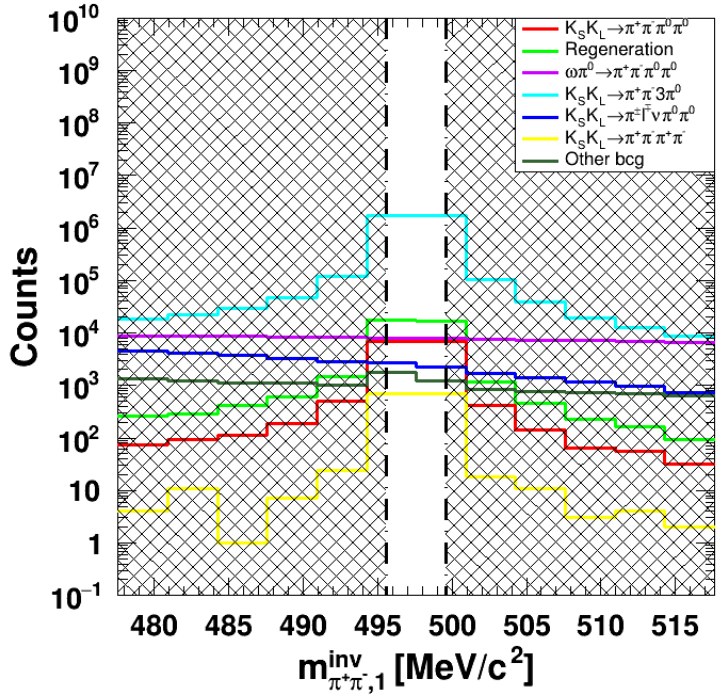

(b) $m^{inv}_{\pi^+\pi^-,1}$ with an indicated rejected region. Bin width is the same w.r.t. Fig. 20.

Fig. 21: Efficiency-purity plots and histogram with indicated rejected regions for $m^{inv}_{\pi^+\pi^-,1}$.

farther from IP. Thus, the definition for $\mathrm{K_S K_L} \to \pi^+\pi^-\pi^+\pi^-$ is:

$$\Delta t_{\mathrm{K_S K_L}\to\pi^+\pi^-\pi^+\pi^-} = t_{\mathrm{K_L}} - t_{\mathrm{K_S}}, \tag{4.14}$$

where the order was chosen arbitrarily. Finally, histograms of proper times of kaons and the Δt distribution can be seen in Fig. 22. Comparison with Fig. 14 reveals, that $\mathrm{K_S K_L} \to \pi^+\pi^-\pi^0\pi^0$ channel is well suppressed, while the most abundant one is $\mathrm{K_S K_L} \to \pi^+\pi^- 3\pi^0$ this will change after the $\mathrm{K} \to \pi^+\pi^-$ cuts. Simultaneously, $t_{\mathrm{K_S}}$ and $t_{\mathrm{K_L}}$ are well separated w.r.t. the lifetimes of kaons. In Fig. 14 they are mixed, which is visible by the peak around zero for both distributions, while here only $t_{\mathrm{K_S}}$ contains it, $t_{\mathrm{K_L}}$ is spread to longer times.

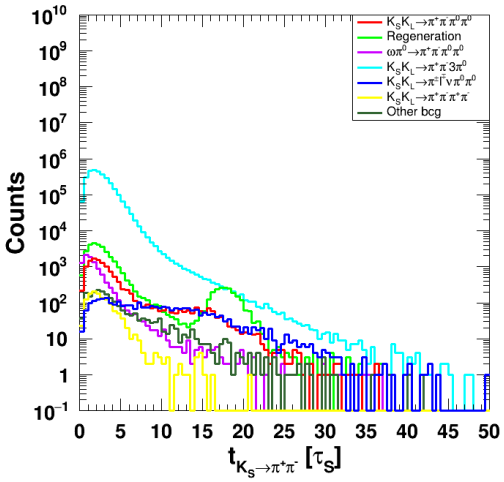

(a) Proper time of kaon from $\mathrm{K_S} \to \pi^+\pi^-$.

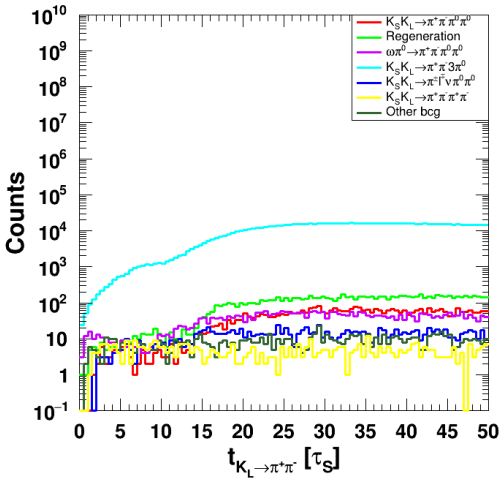

(b) Proper time of kaon from $\mathrm{K_L} \to \pi^+\pi^-$.

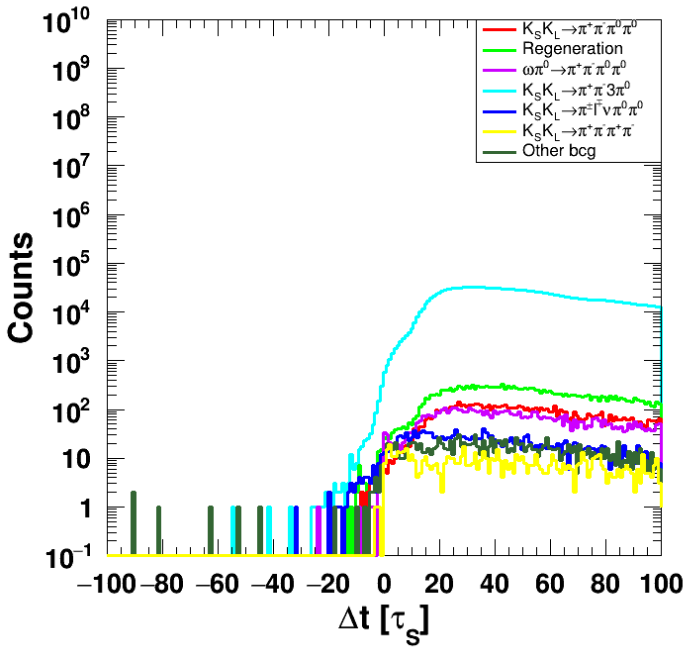

(c) Δt calculated from reconstructed kaons' proper times, specifically for $\mathrm{K_S K_L} \to \pi^+\pi^-\pi^+\pi^-$ using $\mathrm{K_1}$ and $\mathrm{K_2}$.

Fig. 22: Reconstructed kaons' paths and Δt for all channels taken for the analysis after $\mathrm{K_S} \to \pi^+\pi^-$ tagging decay selection.

This point ends the entire selection part and analysis of efficiencies can be started. The next subsection is devoted to separate studies on the efficiencies resulting from control samples along with DATA distributions.

4.3 Efficiency correction measurement and error determination

Beginning from this moment, samples will not be decomposed into individual channels, but will be treated entirely as a properly selected decays for the purpose of efficiency correction. Moreover, these distributions will be fitted to DATA to control the appropriateness of the performed steps w.r.t the shapes of histograms.

The first step is to find the *expected* Δt distribution, basing on assumptions from Table 4 and Table 5. Technically, it comes to the filling of histograms of Δt with weights equal to probabilities assigned in N_{exp} parts of both tables.

As the signal selections have been discussed in the beginning of the section, they have to be imposed now on the corresponding expected distributions of DATA to mimic $\mathrm{K_S K_L} \to \pi^+\pi^-\pi^0\pi^0$ selection performed on MC. Values of selections are kept with respect to the original assumptions. The only difference between control samples selection and efficiency estimated from MC generated $\mathrm{K_S K_L} \to \pi^+\pi^-\pi^0\pi^0$ events is based on $\mathrm{K} \to \pi^0\pi^0$ conditions. Important is, however, how behave the efficiencies for control samples determined from $\mathrm{K_S K_L} \to \pi^+\pi^- 3\pi^0$ and $\mathrm{K_S K_L} \to \pi^+\pi^-\pi^+\pi^-$, respectively. Prediction of their efficiencies in the function of kaon's path length can be found in Fig. 23.

As can be seen, efficiency from $\mathrm{K_S K_L} \to \pi^+\pi^- 3\pi^0$ corresponds to $\mathrm{K_S} \to \pi^+\pi^-$ and the one from $\mathrm{K_S K_L} \to \pi^\pm \mathrm{l}^\mp \nu \pi^0\pi^0$ is compatible with the prediction of $\mathrm{K_L} \to \pi^+\pi^-$ for this control sample. They overlap in the region $\sim$2 cm, so complementary can be used to define the control sample for the total $\mathrm{K} \to \pi^+\pi^-$, as was assumed in the beginning of the analysis.

Finally, the behavior of the efficiency determined from DATA is cross-checked with the efficiency determined from Monte Carlo. The efficiency plot is determined via the combination of sub-efficiencies connected to all control samples. Technically, it was done using `TEfficiency:Combine` - detailed description can be found in [38]. Uncertainties of such a distribution are found basing on the binomial method from [39] in the form:

$$\sigma_{\epsilon,i} = \sqrt{\frac{\epsilon_i(1-\epsilon_i)}{N_i}}, \tag{4.15}$$

where ϵ_i is the estimator of an efficiency and N_i stands for the total number of events in the i-th bin. With the statistics available in these studies, binomially determined errors behave properly and, moreover, are symmetric, which is desired for their propagation in the final result. The final determination of a correction factor was done using Eq. (3.9) on the distribution of efficiency connected with $\mathrm{K_S K_L} \to \pi^+\pi^-\pi^0\pi^0$ selection from MC (gray points)

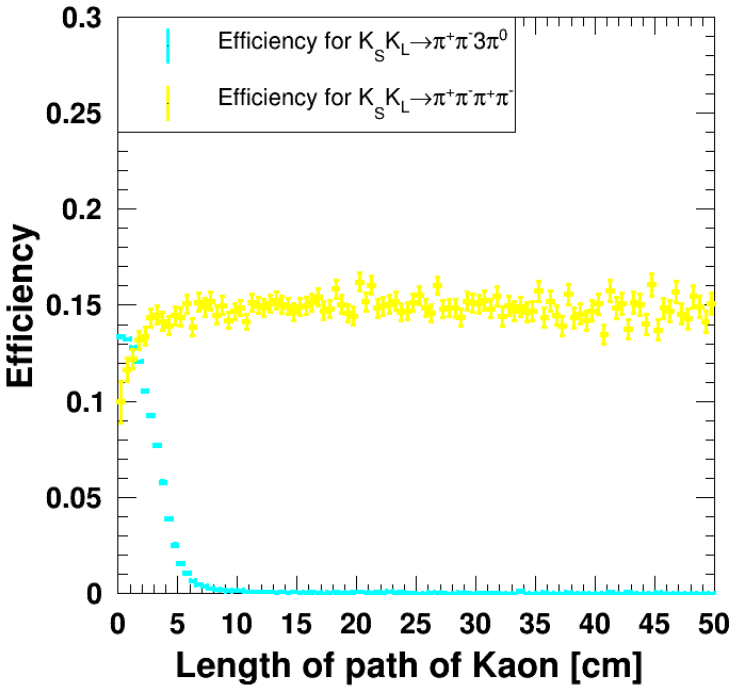

Fig. 23: Comparison of efficiencies for control samples for $\mathrm{K_S} \to \pi^+\pi^-$ (determined from $\mathrm{K_S K_L} \to \pi^+\pi^- 3\pi^0$) and for $\mathrm{K_L} \to \pi^+\pi^-$ (determined from $\mathrm{K_S K_L} \to \pi^{\pm} \mathrm{l}^{\mp} \nu \pi^0 \pi^0$). As can be seen, they overlap around 2 cm length, so jointly can be used to determine an efficiency for $\mathrm{K} \to \pi^+\pi^-$.

and the one determined from DATA (black points), which are visible in Fig. 24a. Thus, literally, it is the division of these two histograms by each other. The final result is visible along with them on Fig. 24b. The efficiencies from Fig. 24a are in good correspondence for the positive side of the Δt axis, while the differences can be noticed for the negative Δt. It proves, that all undertaken selections were controlled well during the analysis from the last subsection, but still exist some differences, which will be corrected using $f(\Delta t)$.

As was mentioned earlier, uncertainty for each point was estimated using a standard propagation of errors, as they do not have mutual correlations. The explicit formula is then:

$$\sigma_i = \sqrt{\left(\frac{1}{\epsilon_i^{MC}} \sigma_{\epsilon^{DATA},i}\right)^2 + \left(\frac{\epsilon_i^{DATA}}{(\epsilon_i^{MC})^2} \sigma_{\epsilon^{MC},i}\right)^2}, \tag{4.16}$$

where i enumerates a bin. The average here was calculated using the formula for a weighted arithmetic mean:

$$\overline{f(\Delta t)} = \frac{\sum_i w_i f(\Delta t)_i}{\sum_i w_i}, \tag{4.17}$$

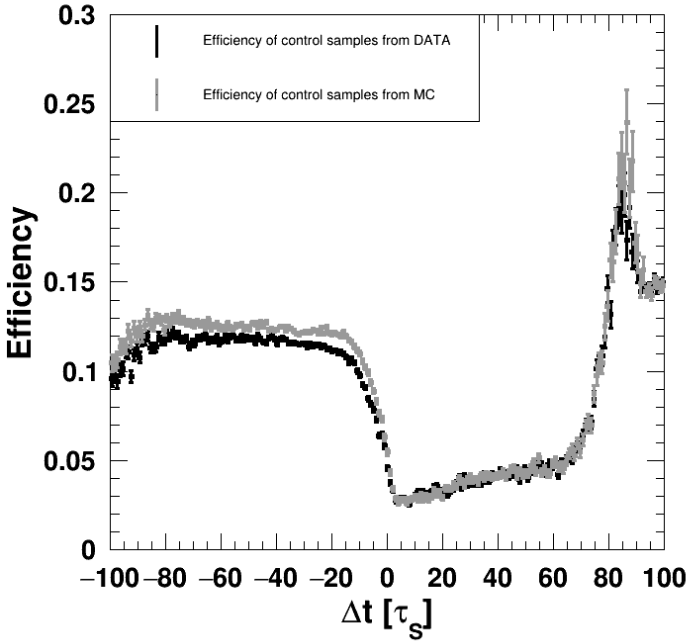

(a) Efficiency calculated for control samples from DATA (black points) and cross-checked with MC control samples (gray points).

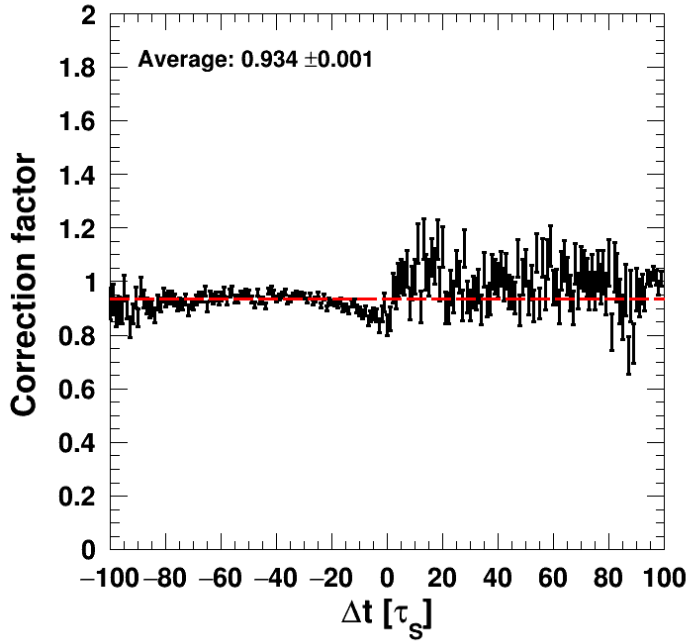

(b) Correction factor determined from DATA. Distribution is non-uniform and uncertainties were estimated using the standard propagation of errors.

Fig. 24: Efficiencies for $\mathrm{K_S K_L} \to \pi^+\pi^-\pi^0\pi^0$ from Monte Carlo cross-checked with the efficiency from DATA and a determined correction factor, which is the final result of this work.

$w_i = 1/\sigma_i^2$ corresponds to the weight of each element. Thus, the standard deviation of this mean is defined by:

$$\sigma_{\overline{f(\Delta t)}} = \sqrt{\frac{1}{\sum_i w_i}}. \tag{4.18}$$

Finally, the average along with its standard deviation is equal to:

$$\overline{f(\Delta t)} = 0.934 \pm 0.001, \tag{4.19}$$

so with a good accuracy it is uniform on the entire range of Δt. It has to be noticed, however, that within $\Delta t \in [-5, 5]\ \tau_S$, where the interference pattern is expected to appear, it varies stronger. It gives the conclusion, that $f(\Delta t)$ should be indeed used independently for each bin, so that the compensation will be much more precise for the further studies of $\mathrm{Re}(\varepsilon'/\varepsilon)$ and $\mathrm{Im}(\varepsilon'/\varepsilon)$.

5 Discussion and summary

Clearly, the main problem in this analysis was the independence between two sides of decays. Using the trilateration resolved it, as it does not take into account momentum of kaon from $\mathrm{K} \to \pi^+\pi^-$ to determine neutral vertex's position. On the other hand, however, the time of flight method for 4γ case provides much better quality of vertices' coordinates. $m_{4\gamma}^{inv}$ found using trilateration could successfully mimic the corresponding variable from the optimized $\mathrm{K_S K_L} \to \pi^+\pi^-\pi^0\pi^0$ selection, but $t_{sum,r}$ has much worse quality in the case of control samples. Due to this fact, the selection of $\mathrm{K} \to \pi^0\pi^0$ from a tagging $\mathrm{K} \to \pi^\pm l^\mp \nu$ will be checked in the further studies.

For the $\mathrm{K} \to \pi^+\pi^-$ control sample, cutting variables were reconstructed using the standard methods with similar qualities. Therefore, this part should constitute the result well controlled and behaving appropriately, taking into account the standard efficiency estimation from Monte Carlo.

To summarize, an additional analysis of the $\mathrm{K} \to \pi^0\pi^0$ control sample is needed to ensure the appropriateness of the determined correction factor. The quality of the trilateration for 4γ case could be improved using the kinematic fit. It should be rebuilt, however, w.r.t the approach from [37] to keep the independence of both reconstructions. Moreover, to improve the purity of $\mathrm{K} \to \pi^\pm l^\mp \nu$ tagging sample, an identification of leptons could be performed to adapt analysis from [40].

Finally, the correction factor behaves properly and uniformly w.r.t the Monte Carlo analysis, so it can be used in the further studies of CP violation in entangled kaons' systems.

Appendices

Appendix A

To derive an interference function visible in Eq. (1.35) one can start with the expression from Eq. (1.32), which, for example, can be found in [17]. Two relations here are, in fact, crucial:

$$\begin{aligned} \eta_1 &\approx \varepsilon + \varepsilon', \\ \eta_2 &\approx \varepsilon - 2\varepsilon'. \end{aligned} \tag{5.1}$$

In the beginning, a trigonometric identity involving angles addition can be used to expand cosine in the form:

$$\begin{aligned} \cos\left(\Delta m \Delta T + (\phi_2 - \phi_1)\right) = \cos\left(\Delta m \Delta T\right)\cos\left(\phi_2 - \phi_1\right) \\ - \sin\left(\Delta m \Delta T\right)\sin\left(\phi_2 - \phi_1\right). \end{aligned} \tag{5.2}$$

Introduction of the upper expression in the Eq. (1.32) and its rearrangement results in:

$$\begin{aligned} I(f_1, f_2; \Delta T \geq 0) = \frac{C_{12}}{\Gamma_S + \Gamma_L}\Bigg[& |\eta_1|^2 e^{-\Gamma_L \Delta T} + |\eta_2|^2 e^{-\Gamma_S \Delta T} \\ & - 2|\eta_1||\eta_2|\cos\left(\phi_2 - \phi_1\right) e^{-\frac{\Gamma_S + \Gamma_L}{2}\Delta T}\cos\left(\Delta m \Delta T\right) \\ & + 2|\eta_1||\eta_2|\sin\left(\phi_2 - \phi_1\right) e^{-\frac{\Gamma_S + \Gamma_L}{2}\Delta T}\sin\left(\Delta m \Delta T\right)\Bigg]. \end{aligned} \tag{5.3}$$

Basing on Eq. (5.1) a formula for ε'/ε can be found:

$$\varepsilon'/\varepsilon = \frac{\eta_1 - \eta_2}{2\eta_1 + \eta_2}, \tag{5.4}$$

but a goal is to find an expression explicitly depending on its real and imaginary parts. It can be achieved by a simplification of a complex number in the denominator to its modulus, which finally gives the results:

$$\begin{aligned} \mathrm{Re}(\varepsilon'/\varepsilon) &= \frac{2|\eta_1|^2 - |\eta_2|^2 - |\eta_1||\eta_2|\cos\left(\phi_2 - \phi_1\right)}{4|\eta_1|^2 + |\eta_2|^2 + 4|\eta_1||\eta_2|\cos\left(\phi_2 - \phi_1\right)}, \\ \mathrm{Im}(\varepsilon'/\varepsilon) &= -\frac{3|\eta_1||\eta_2|\sin\left(\phi_2 - \phi_1\right)}{4|\eta_1|^2 + |\eta_2|^2 + 4|\eta_1||\eta_2|\cos\left(\phi_2 - \phi_1\right)}. \end{aligned} \tag{5.5}$$

This is a set of linear equations for $|\eta_1||\eta_2|\sin\left(\phi_2 - \phi_1\right)$ and $|\eta_1||\eta_2|\cos\left(\phi_2 - \phi_1\right)$, which could be solved using, for example, `Mathematica` [41]. Finally, it is found, that:

$$\begin{aligned} |\eta_1||\eta_2|\sin\left(\phi_2 - \phi_1\right) &= -\frac{4|\eta_1|^2 - |\eta_2|^2}{1 + 4\mathrm{Re}(\varepsilon'/\varepsilon)}\mathrm{Im}(\varepsilon'/\varepsilon), \\ |\eta_1||\eta_2|\cos\left(\phi_2 - \phi_1\right) &= \frac{2|\eta_1|^2 - |\eta_2|^2 - \left(4|\eta_1|^2 + |\eta_2|^2\right)\mathrm{Re}(\varepsilon'/\varepsilon)}{1 + 4\mathrm{Re}(\varepsilon'/\varepsilon)}. \end{aligned} \tag{5.6}$$

$|\eta_1|$ and $|\eta_2|$ have to be found explicitly, before the introduction of these results into the Eq. (5.3). It can be done by manipulations of Eq. (5.1), which give expressions:

$$\begin{aligned} |\eta_1|^2 &= |\varepsilon + \varepsilon'|^2 = |\varepsilon|^2 \left|1 + \frac{\varepsilon'}{\varepsilon}\right|^2 = |\varepsilon|^2(1 + 2\mathrm{Re}(\varepsilon'/\varepsilon) + \left|\frac{\varepsilon'}{\varepsilon}\right|^2), \\ |\eta_2|^2 &= |\varepsilon - 2\varepsilon'|^2 = |\varepsilon|^2 \left|1 - 2\frac{\varepsilon'}{\varepsilon}\right|^2 = |\varepsilon|^2(1 - 4\mathrm{Re}(\varepsilon'/\varepsilon) + 4\left|\frac{\varepsilon'}{\varepsilon}\right|^2), \end{aligned} \tag{5.7}$$

but knowing, that $\left|\frac{\varepsilon'}{\varepsilon}\right|^2$ should be a few orders of magnitude smaller, than the other components it can be neglected, so that:

$$\begin{aligned} |\eta_1|^2 &= |\varepsilon|^2(1 + 2\mathrm{Re}(\varepsilon'/\varepsilon)), \\ |\eta_2|^2 &= |\varepsilon|^2(1 - 4\mathrm{Re}(\varepsilon'/\varepsilon)). \end{aligned} \tag{5.8}$$

These results can be joint and Eq. (5.6) simplified to the final form:

$$\begin{aligned} |\eta_1||\eta_2| \sin(\phi_2 - \phi_1) &= -3|\varepsilon|^2 \mathrm{Im}(\varepsilon'/\varepsilon), \\ |\eta_1||\eta_2| \cos(\phi_2 - \phi_1) &= |\varepsilon|^2 (1 - \mathrm{Re}(\varepsilon'/\varepsilon)). \end{aligned} \tag{5.9}$$

Both Eq. (5.8) and Eq. (5.9) can be applied in the Eq. (5.3) and give the final expression for the interference function, which is used in the entire studies:

$$\begin{aligned} &I(f_1, f_2; \Delta T \geq 0) = \\ &C_{12}\frac{|\varepsilon|^2}{\Gamma_S + \Gamma_L}\Big[(1 + 2\mathrm{Re}(\varepsilon'/\varepsilon))e^{-\Gamma_L \Delta T} + (1 - 4\mathrm{Re}(\varepsilon'/\varepsilon))e^{-\Gamma_S \Delta T} \\ &-2e^{-\frac{\Gamma_S + \Gamma_L}{2}\Delta T}((1 - \mathrm{Re}(\varepsilon'/\varepsilon))\cos(\Delta m \Delta T) + 3\mathrm{Im}(\varepsilon'/\varepsilon)\sin(\Delta m \Delta T))\Big]. \end{aligned} \tag{5.10}$$

Appendix B

After obtaining the reconstructed 4-momentum of kaon from $\mathrm{K} \to \pi^+\pi^-$ decay, it is possible to improve the resolution of energy using *boost method*. It is based on the hypothesis of a 2 body decay $\phi \to \mathrm{K_S K_L}$, so equally it can be used to reject events, which physically do not fulfill this condition, e.g., $\mathrm{K_S K_L} \to \pi^{\pm} l^{\mp} \nu \pi^0 \pi^0$, where the reconstruction of $\mathrm{K} \to \pi^{\pm} l^{\mp} \nu$ is affected by the neutrino's momentum not taken into account.

Due to this assumption, the plane of reaction can be fixed to x-z plane. For the purpose of comfort, x-direction is placed along $\vec{p}_{\phi}^{\,LAB}$, so 4-momentum of the system in LAB is defined by:

$$\mathbf{p}_{\phi}^{\mathrm{LAB}} = \begin{pmatrix} \sqrt{s} \\ ||\vec{p}_{\phi}^{\,LAB}|| \\ 0 \\ 0 \end{pmatrix}, \tag{5.11}$$

so simultaneously kaon's 4-momentum in LAB frame is defined as:

$$\mathbf{p}_{\mathrm{K}}^{\mathrm{LAB}} = \begin{pmatrix} E_{\mathrm{K}}^{LAB} \\ ||\vec{p}_{\mathrm{K}}^{LAB}|| \cos\alpha \\ ||\vec{p}_{\mathrm{K}}^{LAB}|| \sin\alpha \\ 0 \end{pmatrix}, \tag{5.12}$$

where α is an angle between $\vec{p}_{\mathrm{K}}^{LAB}$ and $\vec{p}_{\phi}^{LAB}$ and $||\vec{p}_{i}^{LAB}||$ stands for the value of a spatial momentum of i-th particle. Lorentz transformation to ϕ's CM frame is thus equal to:

$$\Lambda = \begin{pmatrix} \gamma & -\beta\gamma & 0 & 0 \\ -\beta\gamma & \gamma & 0 & 0 \\ 0 & 0 & 1 & 0 \\ 0 & 0 & 0 & 1 \end{pmatrix}, \tag{5.13}$$

where $\beta = ||\vec{p}_{\phi}^{LAB}||/\sqrt{s}$ and $\gamma = 1/\sqrt{1-\beta^2}$. Its manifest application on both 4-momenta gives the actual forms in CM frame:

$$\mathbf{p}_{\phi}^{\mathrm{LAB}} = \begin{pmatrix} \gamma\sqrt{s} - \beta\gamma||\vec{p}_{\phi}^{LAB}|| \\ 0 \\ 0 \\ 0 \end{pmatrix}, \tag{5.14}$$

$$\mathbf{p}_{\mathrm{K}}^{\mathrm{CM}} = \begin{pmatrix} \gamma E_{\mathrm{K}}^{LAB} - \beta\gamma||\vec{p}_{\mathrm{K}}^{LAB}|| \cos\alpha \\ \gamma||\vec{p}_{\mathrm{K}}^{LAB}|| \cos\alpha - \beta\gamma E_{\mathrm{K}}^{LAB} \\ ||\vec{p}_{\mathrm{K}}^{LAB}|| \sin\alpha \\ 0 \end{pmatrix}. \tag{5.15}$$

On the other hand, state is $\mathrm{K_S K_L}$, so for their almost equal masses ($m_{K_L} - m_{K_S} \approx 3.48 \times 10^{-12}$ MeV/c^2 [7]) it kinematically behaves as an event with identical particles. Thus, the 4-momentum of kaon from $\mathrm{K} \to \pi^+\pi^-$ decay is in ϕ's CM frame equal to:

$$\mathbf{p}_{\mathrm{K}}^{\mathrm{CM}} = \begin{pmatrix} (\gamma\sqrt{s} - \beta\gamma||\vec{p}_{\phi}^{LAB}||)/2 \\ \vec{p}_{\mathrm{K}}^{CM} \end{pmatrix}. \tag{5.16}$$

Eq. (5.15) and Eq. (5.16) can be compared, so that:

$$\frac{\gamma\sqrt{s} - \beta\gamma||\vec{p}_{\phi}^{LAB}||}{2} = \gamma E_{\mathrm{K}}^{LAB} - \beta\gamma||\vec{p}_{\mathrm{K}}^{LAB}|| \cos\alpha, \tag{5.17}$$

and explicitly $||\vec{p}_{\mathrm{K}}^{LAB}|| = \sqrt{(E_{\mathrm{K}}^{LAB})^2 - m_{\mathrm{K}_0}^2}$. Both sides of the expression can be squared up and after reordering the terms a quadratic equation for E_{K}^{LAB} is found:

$$\begin{gathered}\gamma^2(1-\beta^2\cos^2\alpha)(E_{\mathrm{K}}^{LAB})^2+\\ \gamma(\beta\gamma||\vec{p}_{\phi}^{LAB}|| - \gamma\sqrt{s})E_{\mathrm{K}}^{LAB}+\\ \frac{1}{4}(\gamma\sqrt{s} - \beta\gamma||\vec{p}_{\phi}^{LAB}||)^2 + \beta^2\gamma^2 m_{\mathrm{K}_0}^2\cos^2\alpha = 0.\end{gathered} \tag{5.18}$$

Parameters of an equation can be identified as:

$$\begin{aligned}A &= \gamma^2(1-\beta^2\cos^2\alpha),\\ B &= \gamma(\beta\gamma||\vec{p}_{\phi}^{LAB}|| - \gamma\sqrt{s}),\\ C &= \frac{1}{4}(\gamma\sqrt{s} - \beta\gamma||\vec{p}_{\phi}^{LAB}||)^2 + \beta^2\gamma^2 m_{\mathrm{K}_0}^2\cos^2\alpha,\end{aligned} \tag{5.19}$$

so the discriminant is equal to:

$$\sqrt{B^2-4AC} = \beta\gamma^2\sqrt{\cos^2\alpha\left((\sqrt{s}-\beta||\vec{p}_{\phi}^{LAB}||)^2 - 4m_{\mathrm{K}_0}^2(1-\beta^2\cos^2\alpha)\right)}. \tag{5.20}$$

Formally, there are two possible solutions in the form:

$$E_{\mathrm{K},1(2)}^{LAB} = \frac{-B+(-)\sqrt{B^2-4AC}}{2A}, \tag{5.21}$$

Here, if discriminant is negative, it is recognized as zero, so only one solution is found according to the equation above. However, if it is positive, an algorithm to decide on physicality of a solution is needed:

- if $E_{\mathrm{K},1(2)}^{LAB} > 0$ and $E_{\mathrm{K},2(1)}^{LAB} < 0$, then the positive one is taken,
- if both solutions are positive, two subcases have to be considered:
  - if $\vec{p}_{\mathrm{K}_0}^{LAB} \cdot \vec{p}_{\phi}^{LAB} > 0$, then $E_{\mathrm{K},1}^{LAB}$ is taken,
  - if $\vec{p}_{\mathrm{K}_0}^{LAB} \cdot \vec{p}_{\phi}^{LAB} < 0$, then $E_{\mathrm{K},2}^{LAB}$ is taken.

The algorithm saturates all possible situations, so for every event it is possible to find a corrected kaon's energy in LAB.

Appendix C

To determine Δt needed for the measurement of interference in the system of entangled kaons, reconstruction of a neutral vertex has to be done. It is based on a so-called *time of flight algorithm*, which will be described below. In fact, due to the lifetime of π^0 ($\tau_{\pi^0} \approx$

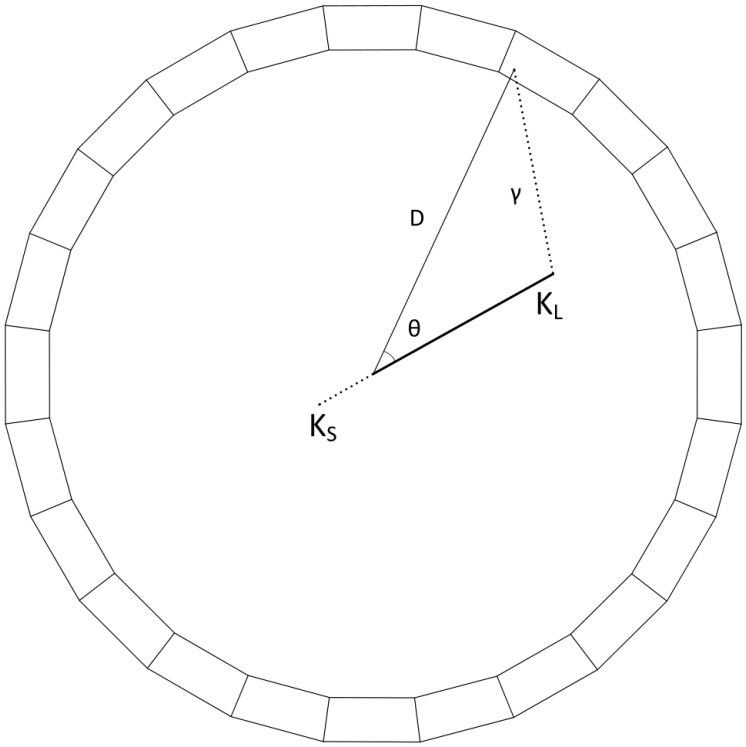

Fig. 25: Scheme of the sought neutral decay. Use of the method is possible even for one registered photon. It is an illustrative scheme method can be used for both $\mathrm{K_{S(L)}} \to \pi^0\pi^0$. Figure adapted from [42].

8.43×10^{-12} ns) measured particles are 4γ, which hit the EMC and their energy and position of clusters can be reconstructed.

The problem here is to find the length of flight path l_K of kaon and finally reconstruct neutral vertex $\vec{V}_\mathrm{neu} = (x_\mathrm{neu}, y_\mathrm{neu}, z_\mathrm{neu})$ using:

$$\begin{aligned} T_{\mathrm{cl},i} &= \frac{l_\mathrm{K}}{\beta_\mathrm{K} c} + \frac{l_{\gamma,i}}{c}, \\ l^2_{\gamma,i} &= \mathrm{D}^2 + l^2_\mathrm{K} - 2\mathrm{D} l_\mathrm{K} \cos\theta, \end{aligned} \tag{5.22}$$

where β_K is a velocity of kaon determined using $\mathbf{p}_{K\to\pi^0\pi^0}$ and the corresponding paths are:

$$\begin{aligned} l_{\gamma,i} &= ||\vec{V}_{\mathrm{cl},i} - \vec{V}_\mathrm{neu}||, \\ l_\mathrm{K} &= ||\vec{V}_\mathrm{neu} - \vec{V}_\mathrm{IP}||, \\ D &= ||\vec{V}_{\mathrm{cl},i} - \vec{V}_\mathrm{IP}||, \end{aligned} \tag{5.23}$$

where $\vec{V}_\mathrm{IP}$ stands for the position of IP. Having l_K determined, coordinates of neutral vertex are found using the formula:

$$\vec{V}_{\mathrm{neu},i} = \frac{\vec{p}_{\mathrm{K}\to\pi^0\pi^0}}{||\vec{p}_{\mathrm{K}\to\pi^0\pi^0}||} l_{\mathrm{K},i}, \tag{5.24}$$

where i stands for the solution found using an i-th cluster. In general, the algorithm uses all events with number of reconstructed clusters ≥ 4, so then the proper set of exactly 4 clusters has to be chosen. For this set, the final $\vec{V}_{\text{neu}}$ is calculated as a weighted average in the form:

$$\vec{V}_{\text{neu}} = \frac{\sum_{i=1}^{4} E_{cl,i}\vec{V}_{\text{neu},i}}{\sum_{i=1}^{4} E_{cl,i}}, \tag{5.25}$$

which takes into account better resolutions of clusters with bigger energy. Finally, it was determined, that the resolution of $\mathrm{K} \to \pi^0\pi^0$ vertex reaches up to $\sim$3 cm using this method quantitative studies and details of the determination can be found in [42].

Appendix D

A method of a neutral vertex reconstruction without use of a 4-momentum of kaon from $\mathrm{K} \to \pi^+\pi^-$ is called *trilateration method* and was developed in [37], initially for 4γ decays. It can be, however, used for 6γ events as well with an extension taking into account all 6 cluster used in [9] analysis.

Mathematically, the method is a search for an intersection point of 4 spheres, each centered at a given cluster's centroid scheme is visible in Fig. 26.

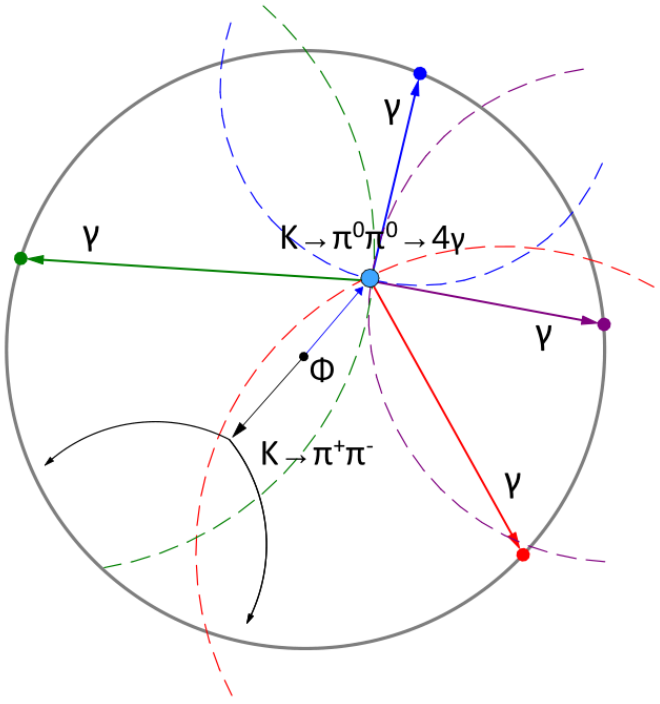

Fig. 26: Illustrative scheme of 4γ decay, with spheres indicated via colored dashed lines. Figure adapted from [37].

Unlike for the time of flight method described in Appendix C, this approach needs all 4 reconstructed clusters. The point of intersection, along with the time of flight of kaon is

found from a system of equations in a form:

$$(X_{cl,i} - x_{neu})^2 + (Y_{cl,i} - y_{neu})^2 + (Z_{cl,i} - z_{neu})^2 = c^2(T_{cl,i} - t_{neu})^2, \tag{5.26}$$

where $i = 1, 2, 3, 4$ is a number of a given cluster. Details corresponding to the solution of the system can be found in [37]. Formally, it gives two, one or no solutions, so due to the numerical character of this issue a set of conditions was established:

- time of flight of kaon has to fit in the range: $t_{neu,n} \in [0, 60]$ ns,
- spatial coordinates of the neutral vertex must lie inside the geometrical limits of the detector, i.e., $\sqrt{x_{neu,n}^2 + y_{neu,n}^2} < 200$ cm and $|z_{neu,n}| < 169$ cm,
- kaon created at IP has to be able to reach neutral vertex with its velocity within the time $t_{neu,n}$,

where $n = 1, 2$ enumerates the solutions. Technically, the first two conditions are strictly geometrical, while the third one is somewhat a crosscheck of solution's correctness. Mathematically, it can be described by:

$$v_{\mathrm{K},n} t_{neu,n} = S_n, \tag{5.27}$$

where $v_{\mathrm{K},n}$ is kaon's velocity for n-th solution and $S_n = ||V_{\mathrm{neu}} - V_{\mathrm{IP}}||$ is a distance covered by kaon from IP to the neutral vertex. As the measurements of properties of given clusters are statistically spread, this condition is not fulfilled exactly, but only to some extent. Thus, for the analysis of this thesis, a strict boundary was chosen as:

$$v_{\mathrm{K},n} t_{neu,n} - S_n < 0.1 \text{ cm}. \tag{5.28}$$

Finally, if only one of the solutions fulfills aforementioned criteria, it is chosen as the physical one. On the other hand, if both fulfill them and $|t_{neu,1} - t_{neu,2}| < 1$ ns - they are recognized as one solution and their arithmetic average is taken to the further analysis. However, if no solution fulfills the conditions, the event is rejected.

Generally, in a given event more than 4 clusters can be reconstructed at one time, so a method to choose an appropriate set has to be mentioned. It is done by checking the compatibility of an invariant mass from a set of clusters taken under consideration with m_{K_0}. The algorithm is iterated over all possible combinations of clusters, and the one with the minimal difference $|m_{4\gamma}^{\mathrm{inv}} - m_{\mathrm{K}_0}|$ is taken for the further analysis.

Finally, a reconstruction of a neutral vertex from 6γ decay has to be explained. It is strictly based on the algorithm described above method to decide on the physical solution is identical, but a choice of the proper set is rather based on a *total error*. For a given set of 6 clusters, it is possible to calculate 15 different solutions for all their combinations from

a system of 4 equations. Then, due to the spread, 15 errors in a form:

$$r_k = \sum_{i=1}^{4} \sqrt{(X_{\mathrm{cl},i} - x_{neu})^2 + (Y_{\mathrm{cl},i} - y_{neu})^2 + (Z_{\mathrm{cl},i} - z_{neu})^2} - c(T_{\mathrm{cl},i} - t_{neu}), \quad (5.29)$$

can be determined and finally their sum:

$$R = \sum_{k=1}^{15} r_k, \quad (5.30)$$

is calculated for each combination of 6 clusters and the proper set minimizes R.

Acknowledgments

I would like to express my warmest gratitude to my supervisor, Dr. Eryk Czerwiński for his knowledge, patience, and support during the entire analysis and preparation of this thesis. Moreover, I would like to thank for giving me the opportunity to work with Him and KLOE on a very early stage of my adventure with academical physics.

I would like to thank Prof. Antonio Di Domenico, Prof. Paolo Gauzzi, Dr. Erika De Lucia and Dr. Antonio De Santis for fruitful meetings, without which preparation of this work would not be possible at the same level.

I am grateful to the entire KLOE-2 collaboration for giving me the opportunity to take part in the kaon working group meetings and General Meetings, which gave me an invaluable experience for the coming scientific life.

I would like to thank my friends, Konrad Pawlik and Mateusz Bajda for the interesting discussions, support and kind words during the whole preparation stage.

Finally, I would like to thank my entire family for their strong support and understanding, and to my fiancée Dominika Bednarz for helping me with Her artistic eyes during the preparation of figures and keeping my sanity at the top.

References

[1] S. Gamrat. Efficiency studies of selection criteria for entangled K mesons in view of ε'/ε ratio determination. Bachelor's thesis, Jagiellonian University, Faculty of Physics, Astronomy and Applied Computer Science, 2021.

[2] E. Noether. Invariant Variation Problems. *Nachrichten von der Gesellschaft der Wissenschaften zu Göttingen, Mathematisch-Physikalische Klasse*, 1918:235–257, 1918.

[3] J. McL. Emmerson. *Symmetry principles in particle physics* . Clarendon Press Oxford, 1972. ISBN 9780198515067.

[4] C. S. Wu et al. Experimental Test of Parity Conservation in Beta Decay. *Phys. Rev.*, 105:1413–1415, Feb 1957.

[5] R. P. Feynman and M. Gell-Mann. Theory of the Fermi Interaction. *Phys. Rev.*, 109: 193–198, Jan 1958. doi: 10.1103/PhysRev.109.193.

[6] G. Culligan et al. Longitudinal Polarization of the Electrons from the Decay of Unpolarized Positive and Negative Muons. *Proceedings of the Physical Society*, 73(2): 169–177, February 1959.

[7] R. L. Workman et al. Review of Particle Physics. *PTEP*, 2022:083C01, 2022.

[8] J. P. Lees et al. Observation of Time Reversal Violation in the B^0 Meson System. *Phys. Rev. Lett.*, 109:211801, 2012.

[9] D. Babusci et al. Direct tests of T, CP, CPT symmetries in transitions of neutral K mesons with the KLOE experiment. 2022.

[10] J. H. Christenson, J. W. Cronin, V. L. Fitch, and R. Turlay. Evidence for the 2π Decay of the K_2^0 Meson. *Phys. Rev. Lett.*, 13:138–140, Jul 1964.

[11] N. Cabibbo. Unitary Symmetry and Leptonic Decays. *Phys. Rev. Lett.*, 10:531–533, Jun 1963.

[12] S. L. Glashow, J. Iliopoulos, and L. Maiani. Weak Interactions with Lepton-Hadron Symmetry. *Phys. Rev. D*, 2:1285–1292, Oct 1970.

[13] J. E. Augustin et al. Discovery of a Narrow Resonance in e^+e^- Annihilation. *Phys. Rev. Lett.*, 33:1406–1408, Dec 1974.

[14] J. J. Aubert et al. Experimental Observation of a Heavy Particle J. *Phys. Rev. Lett.*, 33:1404–1406, Dec 1974.

[15] M. Kobayashi and T. Maskawa. CP Violation in the Renormalizable Theory of Weak Interaction. *Prog. Theor. Phys.*, 49:652–657, 1973.

[16] G. Rochester and C. Butler. Evidence for the Existence of New Unstable Elementary Particles. *Nature*, 160:855–857, 1947.

[17] *Handbook on neutral kaon interferometry at a Φ-factory*, volume 43 of *Frascati physics series*, Frascati, Italy, 2007. INFN.

[18] A. Pais and O. Piccioni. Note on the Decay and Absorption of the θ^0. *Phys. Rev.*, 100:1487–1489, Dec 1955.

[19] L. K. Gibbons et al. Measurement of the CP-violation parameter Re(ε'/ε). *Phys. Rev. Lett.*, 70:1203–1206, Mar 1993.

[20] G. D. Barr et al. A New measurement of direct CP violation in the neutral kaon system. *Phys. Lett. B*, 317:233–242, 1993.

[21] J. R. Batley et al. A Precision measurement of direct CP violation in the decay of neutral kaons into two pions. *Phys. Lett. B*, 544:97–112, 2002.

[22] E. Abouzaid et al. Precise measurements of direct CP violation, CPT symmetry, and other parameters in the neutral kaon system. *Phys. Rev. D*, 83:092001, May 2011.

[23] A. Alavi-Harati et al. Measurements of direct CP violation, CPT symmetry, and other parameters in the neutral kaon system. *Phys. Rev. D*, 67:012005, 2003. doi: 10.1103/PhysRevD.70.079904. [Erratum: Phys.Rev.D 70, 079904 (2004)].

[24] M. Adinolfi et al. The KLOE electromagnetic calorimeter. *Nucl. Instrum. Meth. A*, 482:364–386, 2002.

[25] Paolo Franzini and Matthew Moulson. The Physics of DAΦNE and KLOE. *Annual Review of Nuclear and Particle Science*, 56(1):207–251, nov 2006.

[26] DAΦNE accelerator division webpage. Last accessed 25 April 2023.

[27] M. Adinolfi et al. The tracking detector of the KLOE experiment. *Nuclear Instruments & Methods in Physics Research Section A-accelerators Spectrometers Detectors and Associated Equipment*, 488:51–73, 2002.

[28] J. Lee-Franzini and P. Franzini. A Flavor of KLOE. *Acta Physica Polonica B*, 38(9): 2703, September 2007.

[29] KLOE official webpage. Last accessed 25 April 2023.

[30] M. Incagli. VTXFIN: the KLOE Vertex Finder Algorithm, 1998. KLOE Internal Document, MEMO 147.

[31] A. Balla et al. Status of the cylindrical-GEM project for the KLOE-2 inner tracker. *Nuclear Instruments and Methods in Physics Research Section A: Accelerators, Spectrometers, Detectors and Associated Equipment*, 628(1):194–198, 2011. ISSN 0168-9002. VCI 2010.

[32] M. Cordelli et al. QCALT: A tile calorimeter for KLOE-2 experiment. *Nuclear Instruments and Methods in Physics Research Section A: Accelerators, Spectrometers, Detectors and Associated Equipment*, 617(1):105–106, 2010. ISSN 0168-9002. 11th Pisa Meeting on Advanced Detectors.

[33] M. Cordelli et al. CCALT: A Crystal CALorimeter with Timing for the KLOE-2 upgrade. *Nuclear Instruments and Methods in Physics Research Section A: Accelerators, Spectrometers, Detectors and Associated Equipment*, 718:81–82, 2013. ISSN 0168-9002. Proceedings of the 12th Pisa Meeting on Advanced Detectors.

[34] F. Ambrosino et al. The Event Classification procedures, 2000. KLOE Internal Document, MEMO 225.

[35] G. Cowan. *Statistical data analysis*. 1998. ISBN 978-0-19-850156-5.

[36] F. James. *Statistical methods in experimental physics*. 2006. ISBN 978-981-256-795-6, 978-981-270-527-3.

[37] A. Gajos. A novel algorithm for the $\mathrm{K} \to \pi^0\pi^0 \to \gamma\gamma\gamma\gamma$ decay vertex reconstruction for the KLOE-2 experiment. Master's thesis, Jagiellonian University, Faculty of Physics, Astronomy and Applied Computer Science, 2013.

[38] Documentation of TEfficiency class from CERN ROOT. Last accessed 14 May 2023.

[39] M. Paterno. Calculating efficiencies and their uncertainties.

[40] A. Gajos. *Investigations of fundamental symmetries with the electron-positron systems*. Phd thesis, Jagiellonian University, Faculty of Physics, Astronomy and Applied Computer Science, 2018.

[41] Wolfram Research, Inc. Mathematica, Version 12.3. Champaign, IL, 2021.

[42] S. Di Falco. *Study of neutral decays of K_L^0 mesons with the $KLOE$ detector*. Phd thesis, University of Pisa, 2001.